



## Impacts of nano-clay particles and heat-treating on out-of-phase thermo-mechanical fatigue characteristics in piston aluminum-silicon alloys

H. Bahmanabadi, M. Azadi, A. Dadashi, J. Torkian, M.S.A. Parast

*Faculty of Mechanical Engineering, Semnan University, Semnan, Iran*

*hamed.ba1992@gmail.com*

*m\_azadi@semnan.ac.ir, <http://orcid.org/0000-0001-8686-8705>*

*dadashi.ali@hotmail.com, jabangir.torkian@gmail.com, aqareb@yahoo.com*

G. Winter, F. Grün

*Chair of Mechanical Engineering, Montanuniversität Leoben, Leoben, Austria*

*gerhard.winter@unileoben.ac.at, florian.gruen@unileoben.ac.at*

**ABSTRACT.** In this article, the effect of nano-clay particles and heat-treating on thermo-mechanical fatigue (TMF) behaviors and failures of piston aluminum-silicon (AlSi) alloys was investigated. For this purpose, thermo-mechanical fatigue tests were conducted under out-of-phase (OP) loading conditions. Two loading conditions were checked based on different maximum temperatures (250, 300 and 350 °C) and various thermo-mechanical loading factors (100, 125 and 150%). The minimum temperature was constant in all tests at 50 °C under a heating/cooling rate of 10 °C/s and a dwell time of 5 s. Results showed that the nano-composites had a longer fatigue lifetime, at least 2 times higher, compared to the Al alloy, when the maximum temperature was 250 °C and the thermo-mechanical loading factor was 100%. However, no effective change was seen for the stress value and the plastic strain. At higher maximum temperatures, the change in the material behavior was lower. The fracture analysis by scanning electron microscopy (SEM) demonstrated that both materials had a brittle behavior due to cleavage and quasi-cleavage marks. The damage mechanism was also due to the Si-rich phase and intermetallics, respectively for the crack propagation and the micro-crack initiation.

**KEYWORDS.** Heat-treating, Nano-clay particles, Thermo-mechanical fatigue, Out-of-phase loading, Piston aluminum-silicon alloy.



**Citation:** Bahmanabadi, H., Azadi, M., Dadashi, A., Torkian, J., Parast, M.S.A., Out-of-phase thermo-mechanical fatigue behaviors and failures in piston aluminum-silicon alloys: Effects of heat-treating and nano-clay particles, *Frattura ed Integrità Strutturale*, 65 (2023) 224-245.

**Received:** 07.05.2023

**Accepted:** 08.06.2023

**Online first:** 12.06.2023

**Published:** 01.07.2023

**Copyright:** © 2023 This is an open access article under the terms of the CC-BY 4.0, which permits unrestricted use, distribution, and reproduction in any medium, provided the original author and source are credited.



## INTRODUCTION

Components with high-temperature service conditions, such as cylinder heads and pistons, are subjected to heating and cooling transients during start and stop operations [1]. Repetition of these conditions led to thermal fatigue due to constrained thermal strains. Thermo-mechanical fatigue is caused by thermal and mechanical loading, during which both the stress and temperature change with time. When the maximum tensile strain occurs at peak temperature and the maximum compressive strain occurs at a minimum temperature, the TMF test is considered as “in-phase” (IP). In “out-of-phase” (OP) TMF, the strain and temperature waveforms are phased with a time-shift equal to the half-cycle period. The damage under TMF loading mainly contains fatigue, creep, and oxidation. During OP-TMF testing the oxidation had a drastic influence on fatigue lifetime and the effect of creep mechanism is not considerable [2]. Neu and Sehitoglu [3] proposed a damage rate-based model in which the fatigue damage, oxidation damage, and creep damage were taken into account. Such modeling is out of the scope of this study and will be evaluated in future works. However, the model of Neu and Sehitoglu could be reached in literature [4]. During TMF testing, when the material deformed under the specified strain and the temperature is held constant for a period of time, stress relaxation phenomenon will occur. In both IP-and OP-TMF loadings, the stress relaxation is defined as the difference between the peak compressive stress at the start of dwell time and the compressive stress at the end of dwell time [5]. Such compressive stresses should be considered in the mid-life cycle. As an important note, during tensile loading in OP-TMF testing, stress relaxation would not occur as the temperature is minimum [6]. Considering the operating condition, the pistons should have a good strength to high temperatures, wear, and cyclic loadings. Much researches were done on the strength of Al alloys under LCF and TMF loadings. As a literature review, some articles are presented below. Zhang et al. [7] investigated the effects of different mechanical strains and different temperatures on the IP-TMF lifetime of cylinder head extracted cast Al alloy. They found that increasing the temperature led to a decrease in the stress amplitude and an increase in the cyclic softening. Li et al. [8] inquired about the TMF behavior of piston Al alloys. They figured out that the maximum tensile and compressive stresses rose due to an increase in the mechanical strain range and degraded as the cycle number increased. Azadi and Shirazabad [9] demonstrated the heat treatment effect on cast A356 aluminum alloy under OP-TMF and LCF loadings at different temperatures. They found a considerable influence on mechanical and LCF behaviors by the heat treatment process, especially at room temperature, but no significant effects were observed on TMF lifetime. Wang et al. [10] evaluated the TMF behaviors and damage mechanisms of AlSi piston alloy at different temperatures. They claimed that the rapid cyclic softening occurred in the initial stage and then the cyclic stress was stable at lower strain amplitudes, but the cyclic stress displayed a gradual decrease up to the final failure at higher strain amplitudes. Natesan et al. [11] assessed the effects of dwell time on the TMF behavior of A356-T7+0.5wt.%Cu alloy used in high specific power combustion engine cylinder heads. They found that the dwell time had no considerable influences on the cyclic behavior and fatigue lifetime of the material. Merhy et al. [12] characterized the crack growth of the A356-T7 alloy under TMF loading. Their experimental results revealed that the decrease in the frequency caused a significant increase in the crack growth rate, especially at high temperatures and load ratios. Azadi et al. [13] presented the effect of a thermal barrier coating layer on OP-TMF lifetime of a diesel engine cylinder head AlSiMg alloy at different maximum temperatures and thermo-mechanical loading factors. They claimed a significant increase in the TMF lifetime of the coated specimens. Azadi [14] investigated the effect of T6 heat treatment on TMF behaviors of A356 aluminum alloy and AZE911 magnesium alloy. Results showed that heat treatment had no significant effects on TMF lifetime of A356 aluminum alloy at the maximum temperature of 250 °C due to the over-ageing phenomenon and against, drastically influenced on TMF lifetime of AZE911 alloy. Fischer and Schweizer [15] assessed the TMF behavior of cylinder head and piston Al alloy. They concluded that the dwell time led to a fast stress relaxation and also showed a negligible effect on the TMF lifetime at maximum temperature. Beck et al. [16] characterized the effect of 15 vol. % discontinuous Al<sub>2</sub>O<sub>3</sub> fibers on the TMF behavior of AlSi10Mg0.3 and AlSi10Mg0.6 alloys at different temperatures. They indicated that both unreinforced alloys had nearly the same lifetime and cyclic deformation behavior. They also depicted that all materials softened cyclically due to over-ageing of the peak-aged matrix alloys. Khisheh et al. [17] investigated the effects of heat treatment and over-ageing process on OP-TMF behaviors of cylinder head AlSiCu alloy. They figured out that the T6 heat treatment improved the fatigue lifetime of non-over-aged alloys drastically and had no considerable influences on the over-aged alloys. Azadi [18] demonstrated the effects of strain rate and mean strain on the OP-TMF and LCF lifetime of AlSi alloys. Experimental results revealed that high-temperature LCF lifetime was more than OP-TMF lifetime due to severe conditions under TMF loadings with variable temperatures. Wang et al. [19] presented the TMF behaviors and corresponding damage mechanisms of AlSi piston alloy at various temperatures under different thermo-mechanical loading factors. They reported that the IP-TMF lifetime was longer than that of OP-TMF except for the higher thermo-mechanical loading factor, and the TMF lifetime decreased with the increasing absolute value of the thermo-mechanical loading factor. Bose-Filho [20] evaluated the LCF and TMF behavior of AlSi cast alloys obtained from different

processes. Experimental results showed that porosity, especially large and irregular pores, provided the main factor in decreasing the fatigue properties of the tested alloys. Wagner et al. [21] demonstrated the OP-TMF behavior and crack initiation of lost foam cast AlSi cylinder heads. They claimed that the TMF caused positive mean stress and also cyclic softening in the material due to the ageing phenomenon. They also alleged that the pore networks are critical for crack initiation. Takahashi and Sasaki [22] conducted the TMF tests on T6 heat-treated A356 aluminum alloy with different ageing conditions. They found that increasing the ageing time and also tempering, led to longer fatigue lifetime. Grieb et al. [23] demonstrated the lifetime of various near-component-shaped cast Al alloys used in diesel engine cylinder heads with different heat treatments under closely-matched TMF loading to the real component loading condition. They found that the ageing temperature had a high effect on AlSi7Mg-T6 alloy and a low effect on the AlMg3Si1(Sc, Zr)-T5. In addition, AlSiCu alloys had higher resistance against the TMF crack initiation.

According to the literature review, a lot of experimental research has been done to investigate the effects of mechanical strain, temperature, heat treatment, ageing conditions, dwell time, material production method, strain rate, mean strain, the addition of particles to the base alloy, coating, etc. on the TMF behaviors of Al alloy. Some researchers also performed the IP-TMF and OP-TMF tests on the piston and/or cylinder head Al alloys to evaluate the effect of thermal and mechanical loadings. However, articles about the nano particles addition to the base alloy are still rare. The novelty of this research is to investigate using of both heat treatment and nano-clay particles on the TMF behavior of piston AlSi alloy were investigated. This research is alongside the previous work about the investigation of the effect of heat treatment and nano-clay particles on the LCF behavior of piston Al alloy.

## MATERIALS AND METHODS

The piston AlSi alloy (with the commercial name of AlSi12CuNiMg) used in this research was made by the gravity casting method. The chemical composition of such an alloy is represented in Tab. 1. Reinforced specimens by nano particles were produced by the stir-casting technique. For such purpose, 1% wt. montmorillonite K-10 nano-clay particles were added to the Al matrix. It is interesting to note that the base material, AlSi, was as the same for both unreinforced and reinforced specimens. As reported in literature [14], the heat treatment mainly changes the microstructure morphology as well as the ductility of the material due to the spheroidizing of Si particles of the material. Notably, the ductility of material was changed according to the results of tensile tests reported in the results section. Indeed, the heat treatment could convert the Si particles to spheroidized Si particles [24]. Such effect would be realized through the solution treatment [25]. Thus, a T6 heat treatment containing 1 hour solution at 500 °C with water-quenching and 2 hours ageing at 300 °C with air-quenching was applied on nano-composites specimens. Such heat treatment procedure was optimized based on the hardness [26] and microstructure improvement, cost-efficiency in industrial applications (solutioning time optimization), and also considering the LCF lifetime at 300 °C (ageing temperature optimization) [27]. Notably, AlSi was the non-heat-treated specimen and AlSi\_N\_HT6 was the heat-treated and reinforced specimen with nano-clay addition. A schematic of applied heat treatment on the nano-composites is illustrated in Fig. 1. More details about specimen production could be reached in literature [27].

It is worth noting that in this article, the notation of "AlSi" shows the unreinforced Al alloy and "AlSi\_N\_HT6" refers to reinforced Al alloy by nano-clay particles and heat treatment.

The microstructural observation of AlSi and AlSi\_N\_HT6 using optical microscopy is demonstrated in Fig. 2. In this figure, the Al matrix, Si, and intermetallics could be observed. The intermetallic phase is containing Mg, Fe, Cu, Ni, etc. which improve the mechanical properties of the material, especially at higher temperatures [28]. The intermetallic phase is coherent to the Al matrix which is beneficial for the mechanical properties due to the strengthening mechanism [29]. According to literature [30], there are three major intermetallics groups in the base alloy (AlSi); Fe-base particles ( $\beta$ -Al<sub>5</sub>FeSi and  $\alpha$ -Al<sub>15</sub>(Mn, Fe)<sub>3</sub>Si<sub>2</sub>), Cu-based intermetallics (Al<sub>2</sub>Cu and AlSiCuMg), and phases containing Ni (Al(NiCuFe)Si and Al(CuNi)Si). The Si particles and intermetallics had higher elastic modulus and hardness compared to the Al matrix [31] which have a considerable effect on the elevated-temperature mechanical properties [32].

Al	Si	Cu	Mg	Ni	Fe	Zn	Mn
83.30	12.70	1.16	1.00	0.80	0.56	0.16	0.12

Table 1: AlSi alloy chemical composition (wt%)

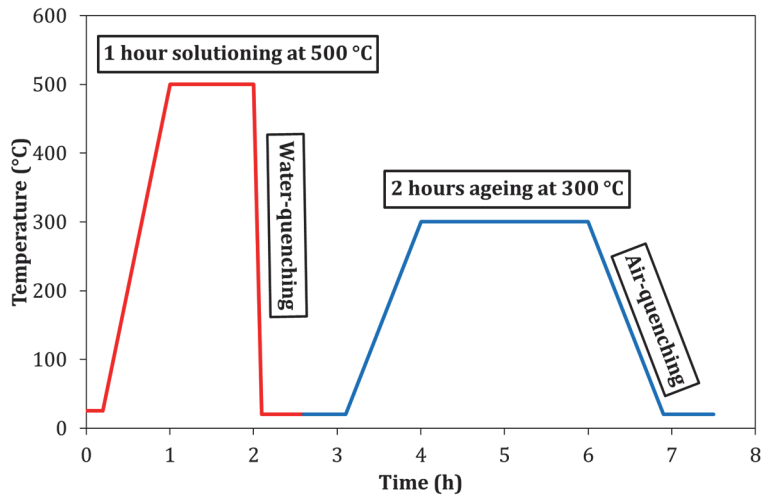
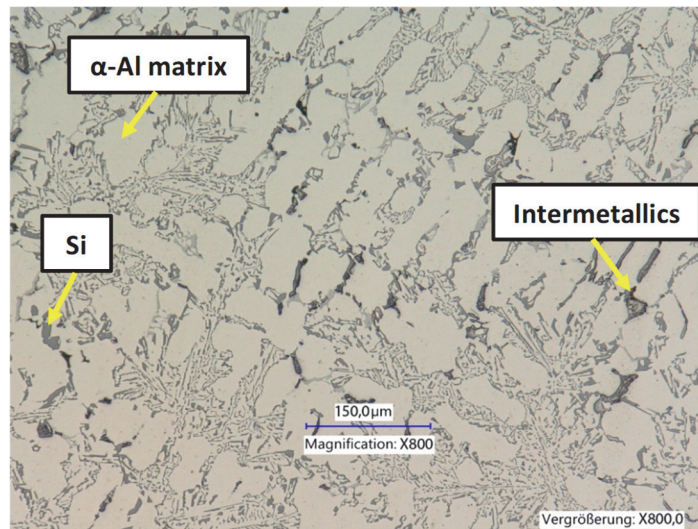
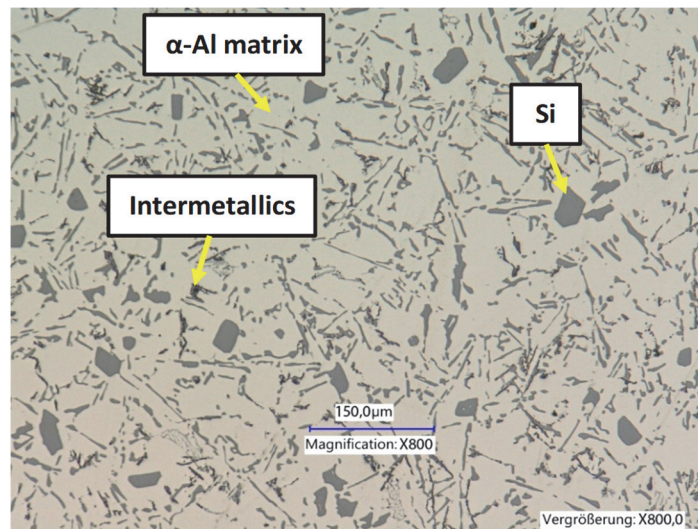


Figure 1: Schematic of applied heat treatment on the nano-composites



(a)



(b)

Figure 2: Microstructure images of (a) AlSi and (b) AlSi\_N\_HT6 using optical microscopy

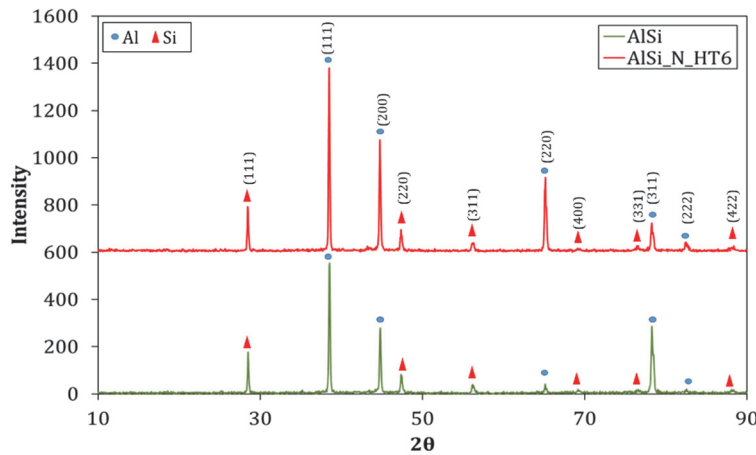


Figure 3: X-ray diffraction analysis (XRD) of AlSi and AlSi\_N\_HT6

The intermetallics had more influences on the properties of the piston AlSi alloy at higher temperatures due to their temperature stability and mechanical properties [33]. Changing the size and morphology of Si had a considerable effect on the mechanical properties [29]. As seen in this figure, the dispersed distribution of Si particles and intermetallic phase improved and became homogeneous in the matrix as the material was reinforced by the nano-clay particles and also heat-treated. Additionally, the size of Si particles increased due to the reinforcement by nano particles and heat treatment. It was expected, as the chemical composition of nano-clay contains 51% of SiO<sub>2</sub>, approximately [27]. Moreover, the acicular-like Si particles accumulated and became blocky-shaped after the reinforcement.

The results of X-ray diffraction analysis (XRD) for reinforced and unreinforced specimens are depicted in Fig. 3. As seen in this figure, Si had the highest value on both specimen surfaces. It was found that no considerable changes were occurred in the materials phases. Hence, the nano-clay as the nucleation particles changed the preferred orientation.

In this research, OP-TMF tests were carried out based on the ISO-12111 standard [34] for strain-controlled TMF testing method using  $\pm 50$  kN servo hydraulic Instron-PLL50K TMF test rig with water-cooled mechanical grips. The load was measured using  $\pm 63$  kN Instron-2326-807 structural testing precision load cell. In order to measure the temperature of specimen surface and hold it constant at the maximum/minimum temperatures during TMF testing, three thermocouples were used. A 10-kW medium-frequency induction generator was used for heating up and a 9-bar compressed air jet was used for cooling down the specimen.

A class 1 Sensotec K-type Sheath thermocouple was inserted in a hole with the diameter of 1.5 mm in order to measure and control the temperature of the center of sample. For measuring the strain during TMF testing, a  $\pm 1.6$  mm MTS 632.53F-14 extensometer with a gauge length of 12.6 mm was used. A computer program was used for control, operation, and data acquisition. Besides, an industrial control B&R 2005 with programmable logic control was used in the Lab View 8.5 for the visualization. The geometry of standard specimens for TMF testing is demonstrated in Fig. 4. In OP-TMF tests, when the temperature increases to its maximum value, the strain has its maximum compressive value and vice versa, as mentioned before. When the temperature has reached its maximum value, it is held for a certain time which is called dwell time ( $t_d$ ). Fig. 5 (a) shows the phase difference between the temperature and mechanical strain. In Fig. 5 (b), the deviation of measured temperature by three surface thermocouples and the sheath thermocouple at the maximum temperature of 250 °C is presented. As seen in this figure, the sheath thermocouple measured the temperature of the specimen inside as 250 °C. Likewise, the temperature of specimen surface measured by middle thermocouple was close to 250 °C. The top and bottom thermocouples show the temperature of specimen surface about 244 °C.

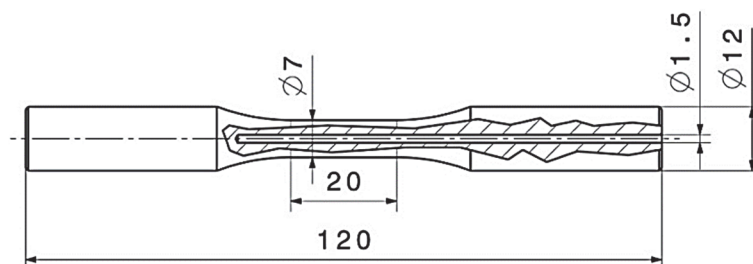


Figure 4: The geometry of the standard specimen for TMF testing

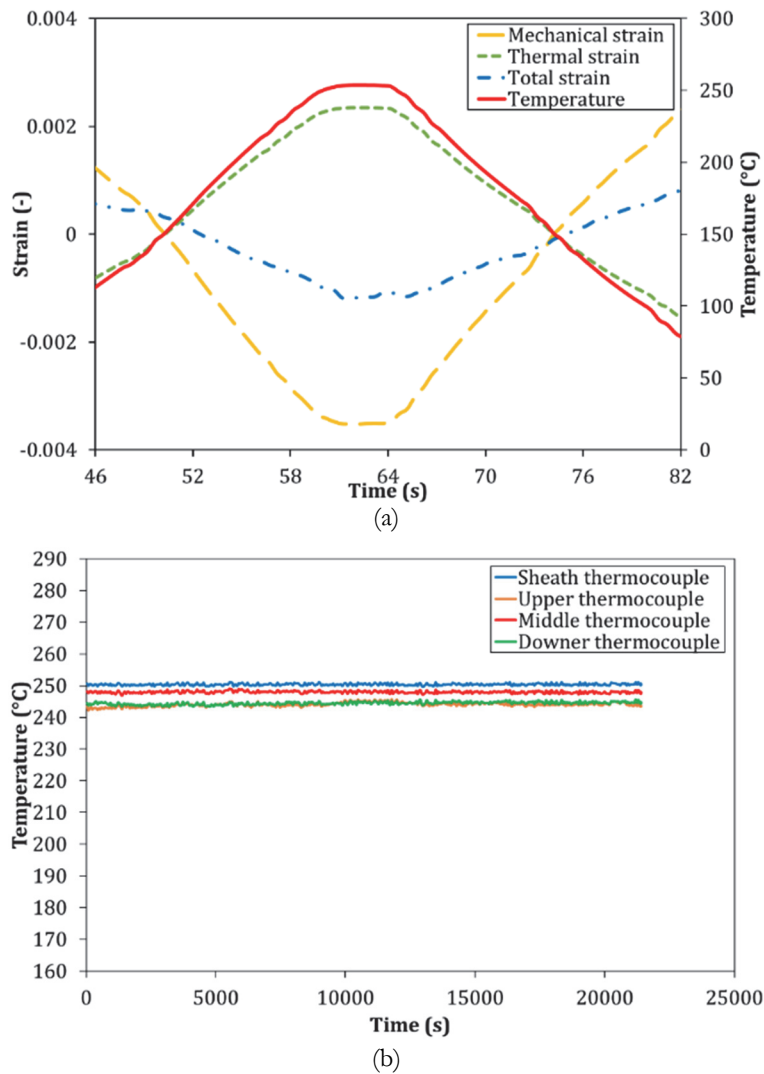


Figure 5: (a) The OP-TMF loading condition and (b) deviation of measured temperatures using different thermocouples, at the maximum temperature of 250 °C.

When a component experienced a temperature gradient, a part of mechanical strain may be occurred by the limitation of the thermal expansion due to the local thermal gradients [35]. For thermal fatigue of the piston, the mechanical strain is dependent on thermal strain and also the local constraint condition of the structure [19]. Thus, the thermo-mechanical loading factor (constraint factor) was introduced in order to evaluate the relationship between mechanical strain and thermal strain during TMF tests [36]. The constraint TMF testing suggests a simple method in order to simulate a complicated operating condition under a constant  $K_{TM}$  which allows more accurate fatigue lifetime prediction under service conditions for the components [19]. The constraint TMF tests are important techniques to evaluate AlSi alloys performance with different production processes such as heat treatment [9], casting process, etc. Eqn. (1) is proposed the thermo-mechanical loading factor [9], as follows:

$$K_{TM} = \frac{\Delta \varepsilon_{a,mech}}{\Delta \varepsilon_{a,th}} = \frac{\Delta \varepsilon_{a,mech}}{\alpha_{th} \Delta T} = \frac{\varepsilon_{mech,(at T=T_{max})} - \varepsilon_{mech,(at T=T_{min})}}{\alpha_{th} (T_{max} - T_{min})} \quad (1)$$

where  $\Delta \varepsilon_{mech}$  is the mechanical strain range,  $\Delta \varepsilon_{th}$  is the thermal strain range,  $\Delta T$  is the temperature range, and  $\alpha_{th}$  is the coefficient of thermal expansion. It should be pointed out that at the first step of each test, the thermal strain was measured using a zero-force test (one cycle with thermal loading and without mechanical loading). Afterward, the coefficient of thermal expansion was measured by the regression method. The mechanical strain was controlled in order to keep the thermo-mechanical loading factor constant.

To investigate the effect of nano-clay particles and heat treatment on the TMF lifetime of AlSi alloy, tension-compression TMF tests were carried out under  $T_{max}=250\text{ }^{\circ}\text{C}$ ,  $300\text{ }^{\circ}\text{C}$  and  $350\text{ }^{\circ}\text{C}$ ,  $K_{TM}=100\%$  and  $t_d=5\text{ s}$ . The maximum temperatures of TMF tests were chosen based on the operating temperature ranges of diesel pistons which are  $250\text{ }^{\circ}\text{C}$ - $400\text{ }^{\circ}\text{C}$  [37]. The minimum temperature was  $50\text{ }^{\circ}\text{C}$  and the heating/cooling rate was  $10\text{ }^{\circ}\text{C/s}$ . It is worth noting that each test was started at the mid-temperature  $(\frac{T_{max} + T_{min}}{2})$ . Besides, to characterize the effect of thermo-mechanical loading factor on TMF lifetime,

fatigue tests were also performed under  $T_{max}=250\text{ }^{\circ}\text{C}$ ,  $K_{TM}=100\%$ ,  $125\%$  and  $150\%$  and  $t_d=5\text{ s}$ . More details about the TMF tests carried out in this research are represented in Tab. 2.

It is interesting to note that the dwell time had no considerable influences on the cyclic behavior and fatigue lifetime of the material under TMF testing [5, 14]. In addition, the mechanical strain rate was  $10^{-4}\text{ 1/s}$ , approximately, and the loading was as a triangular waveform. In each test, the first drop in maximum stress during fatigue cycles was chosen as the TMF failure. Based on this method (tensile force drop), the specimen is considered to be failed when 5-50 percent of the force, drops down from the previously recorded peak force [38]. As another reference, COP-EUR22281EN standard [39], the failure of specimen is occurred when the maximum stress during fatigue cycles drops between 10-50%.

## RESULTS AND DISCUSSION

As the first result, tensile properties of the base alloy and reinforced specimen are illustrated in Fig. 6. For quantitative observation, mechanical properties of both materials are represented in Tab. 3. It is obvious that increasing the temperature led to decrease in the ultimate tensile strength ( $\sigma_{ut}$ ), yield stress ( $\sigma_{yt}$ ), and elastic modulus ( $E$ ) of both materials which was also reported in literature [40]. Such phenomenon is due to instability of the phases containing Ni, Mg and Cu particles [41]. Against, as the temperature increased, the elongation ( $\epsilon$ ) of AlSi and AlSi\_N\_HT6 also increased. Accordingly, the reinforcement also caused to decrease in the  $\sigma_{ut}$  and  $E$  of the material at  $25\text{ }^{\circ}\text{C}$  and  $250\text{ }^{\circ}\text{C}$ . However, at the temperature of  $300\text{ }^{\circ}\text{C}$ , the nano-clay and heat treatment had no considerable influences on the  $\sigma_{ut}$  of material. At  $25\text{ }^{\circ}\text{C}$  and  $250\text{ }^{\circ}\text{C}$  the reinforcement caused to increase in the  $\sigma_{yt}$  and did not affect the  $\sigma_{yt}$  at  $300\text{ }^{\circ}\text{C}$ . The results of tensile tests showed that the reinforcement and also increasing the temperature changed the ductility of material and make the material behave more ductile. As reported in literature [42], the general influences of increasing the temperature were to increase the ductility of material.

### Maximum Temperature Effect

The objective of this research was to investigate the effect of maximum temperature on the OP-TMF behavior of piston AlSi alloy and metal-matrix nano-composites. Stress and strain behaviors of both materials during fatigue cycles under  $K_{TM}=100\%$  and  $t_d=5\text{ s}$  are reported in Fig. 7.

Results of OP-TMF testing for AlSi and AlSi\_N\_HT6 at  $T_{max}=250\text{ }^{\circ}\text{C}$  are depicted in Fig. 7 (a-c). According to this figure, after an initial hardening, a slight decrease was seen in the stress amplitude of AlSi during the TMF cycles, which means that cyclic softening occurred for the base alloy at  $250\text{ }^{\circ}\text{C}$ , similar to literature [15], which reported a negligible cyclic softening for a piston AlSi alloy at the temperature of  $250\text{ }^{\circ}\text{C}$ . The formation of Al-rich phases decreases the elastic modulus of the material, which caused initial hardening under lower strain amplitudes [43]. Indeed, the dislocations increased by the initial hardening without the interaction of Si particles [43]. Although not considerable variations were seen in the stress amplitude of AlSi\_N\_HT6 which means that the reinforcement did not affect the cyclic behavior of the nano-composites.

TMF testing conditions	Objective	
	$T_{max}$ effect	$K_{TM}$ effect
Maximum temperature: $T_{max}$ ( $^{\circ}\text{C}$ )	250, 300, 350	250
Minimum temperature: $T_{min}$ ( $^{\circ}\text{C}$ )	50	50
Heating/Cooling rate ( $^{\circ}\text{C/s}$ )	10	10
Thermo-mechanical loading factor: $K_{TM}$ (%)	100	100, 125, 150
Hold time or dwell time: $t_d$ (s)	5	5

Table 2: Details of TMF testing on AlSi and AlSi\_N\_HT6.

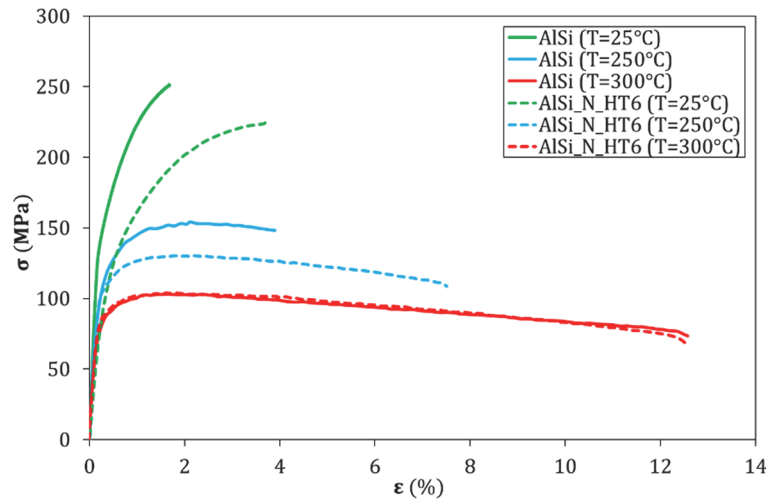


Figure 6: Tensile test results of AlSi and AlSi\_N\_HT6 at different temperatures.

Material type	$T$ (°C)	$\sigma_{ut}$ (MPa)	$\sigma_{yf}$ (MPa)	$e$ (%)	$E$ (GPa)
AlSi	25	251.03	115.80	1.68	82.09
	250	153.18	99.29	3.89	74.70
	300	103.11	79.91	12.37	64.66
AlSi_N_HT6	25	224.40	99.12	3.69	70.53
	250	130.14	96.51	7.50	63.78
	300	103.70	79.79	12.45	58.61

Table 3: Tensile properties of AlSi and AlSi\_N\_HT6 at the temperatures of 25 °C, 250 °C and 300 °C

As seen in this figure, the TMF lifetime of AlSi\_N\_HT6 was about 668 cycles more than that of AlSi. A reason for the difference between the TMF lifetime of reinforced and unreinforced specimens could be the casting defects in the unreinforced specimen which were observed and reported in the fracture surface of specimens in previous work [27]. These defects such as voids and pores could cause a stress concentration [44], which led to a decrease in the fatigue lifetime [45]. Another reason for the diversity of the fatigue lifetime was due to the effect of reinforcements on the TMF lifetime of AlSi alloys under this testing condition. However, for the verification of the results, more fatigue tests are needed to be performed under  $T_{max}=250$  °C,  $K_{TM}=100\%$ , and  $t_d=5$  s. As reported in literature [46] morphologies and size of precipitates could influence Al alloys under monotonic and cyclic loadings. Furthermore, well-dispersed precipitates could improve fatigue behavior and also crack initiation of Al alloys [47]. As also reported in literature [48], the reinforcement with small particles could decrease the strain localization which is mainly determinative of fatigue lifetime. From Fig. 7 (a-c), it was also seen that the plastic strain of AlSi increased during TMF cycles. Although the plastic strain of AlSi was more than that of the one for AlSi\_N\_HT6, the differences were less than 15% and thus, the reinforcement of the Al alloy with nano-clay particles and heat treatment could not be assumed as an effective parameter on the plastic strain of the alloy at 250 °C.

Fig. 7 (d-f) shows the maximum and minimum stress, the stress amplitude and mean stress, and the plastic strain of AlSi and AlSi\_N\_HT6 during fatigue cycles at  $T_{max}=300$  °C. It is interesting to note that  $K_{TM}=100\%$  and  $t_d=5$  s. As seen in this figure, the stress was dropped down before the final failure of the material, which is due to the decohesion of the Si particles [43]. The stress amplitude of both specimens decreased during fatigue cycles and means that cyclic softening occurred. According to this figure, a rapid cyclic softening occurred for AlSi during the first 100 TMF cycles followed by a slight softening until failure which was a match with the results reported in literature [49]. Additionally, the rate of cyclic softening for both specimens at the maximum temperature of 300 °C increased compared to the TMF testing at 250 °C. According to literature [9, 17], the rate of cyclic softening for Al alloys would be enhanced as the temperature raised. Although the stress amplitude of AlSi and AlSi\_N\_HT6 had the same value in the first cycle, the amount of stress decrement for AlSi\_N\_HT6 was higher than that of AlSi which shows a higher rate of cyclic softening for the reinforced specimen. It was due to the over-ageing phenomenon for AlSi\_N\_HT6 at 300 °C which was equal to the ageing treatment temperature [14]. Such results were a match with literature [50] which revealed that materials will be over-aged at the temperatures higher than

150 °C. This phenomenon is due to the formation of specific intermetallics or eutectic phases such as Si with magnesium, iron, or copper in the microstructure [50]. Moreover, increasing the Si content in the material which was about 51% of a compound constituent of nano-clay particles could increase the rate of cyclic softening [27, 51]. Higher values of stress amplitude and lower values of plastic strain for the reinforced specimen showed that reinforcement imposed a brittle behavior on the material. The fatigue lifetime of base alloy was just about 200 cycles more than that of the reinforced specimen which means that the heat treatment and nano particles had no significant effect on the TMF lifetime of the material. It is interesting to note that after about 1500 cycles the stress amplitude of both materials was considered near each other. Such behavior was due to microstructural changes at the maximum temperature of 300 °C which was equal to the ageing temperature [9]. In other words, such microstructural changes were caused by the over-ageing phenomenon [52]. This over-ageing was more pronounced at higher temperatures and lower strain rates, where the solute atoms have the opportunity to precipitate in the Al matrix [52]. As mentioned before, the mechanical strain rate was about  $10^{-4}$  1/s, which enhanced the potential of the cyclic softening of heat-treated material due to the over-ageing phenomenon [53]. Moreover, the strain rate has more effect on TMF lifetime [15].

Fig. 7 (g-i) shows the results for AlSi and AlSi\_N\_HT6 including maximum and minimum stress, stress amplitude and mean stress, and plastic strain during fatigue cycles under  $T_{max}=350$  °C,  $K_{TM}=100\%$  and  $t_d=5$  s. As seen in this figure, the stress amplitude of reinforced specimen was higher than that of the base alloy. However, a reverse behavior was seen in the plastic strain of AlSi and AlSi\_N\_HT6 which means that at the maximum temperature of 350 °C the reinforced specimen had a brittle behavior. Albeit, the stress amplitude of AlSi\_N\_HT6 decreased during the TMF cycles which shows the cyclic softening behavior of such nano-composites. A reason for the stress reduction during fatigue cycles could be the small fatigue crack growth which causes to cyclic softening of the material. As regards, considering Fig. 7 shows that such behavior was repeated for the material at different temperatures. Moreover, according to the results obtained in our previous work [27], both AlSi and AlSi\_N\_HT6 experienced cyclic softening during fatigue cycles at high temperatures which means that the cyclic softening of the materials is related to the microstructural behavior. According to Fig. 7 (h) a rapid cyclic softening occurred for AlSi\_N\_HT6 during the first 20 cycles and the rate of cyclic softening decreased during the TMF cycles until the final fracture. Such a similar behavior was observed for the reinforced AlSi alloy under TMF testing in literature [51]. However, no considerable variations were seen for the stress amplitude of AlSi during fatigue lifetime. It could be mentioned that the reinforcement did not affect the fatigue lifetime of the Al alloy since the fatigue lifetime of AlSi was about 20 cycles higher than that of AlSi\_N\_HT6. Higher stress amplitude and lower plastic strain for the heat-treated nano-composites illustrate that the heat treatment made the material behave in a brittle manner, as also reported by Azadi [14]. Higher stress levels for the reinforced specimens were also reported in literature [51] which was due to increasing the Si content in the material composition. Compared to TMF testing at the maximum temperature of 250 °C and 300 °C, the TMF lifetime of both reinforced and unreinforced specimens decreased as the maximum temperature increased to 350 °C. It was concluded that the TMF testing temperature predominated the influences of ageing treatment as the testing temperature was higher than that of the ageing temperature [9]. Considering Fig. 7 shows a stress reduction with increasing temperature, which means that the mechanical strength of the material decreased. Such behavior was also reported in literature [15]. The stress was gradually decreased from the maximum temperature 150 °C to 250 °C and also from the maximum temperature 250 °C to 350 °C [15]. Indeed, as the material microstructure influences the crack initiation, the crack propagation and the fatigue lifetime are dependent on the temperature and loading conditions [15].

Comparing the results of TMF testing at the maximum temperatures of 250 °C, 300 °C, and 350 °C with  $K_{TM}=100\%$  and  $t_d=5$  s, showed that the fatigue lifetime of both materials increased at the maximum temperature of 300 °C. Such an increment was due to the over-ageing phenomenon [54], which caused microstructural changes in the materials [13]. It was inferred from increasing the TMF lifetime of AlSi and AlSi\_N\_HT6 that the optimum temperature for both materials under TMF testing was 300 °C.

In Fig. 8, the hysteresis loops of AlSi and AlSi\_N\_HT6 under  $T_{max}=250-350$  °C,  $K_{TM}=100\%$  and  $t_d=5$  s are presented. Moreover, Fig. 9 depicts the results of maximum and minimum stresses, the stress amplitude and the mean stress, plus the plastic strain versus TMF lifetime for AlSi and AlSi\_N\_HT6, under  $T_{max}=250$  °C,  $K_{TM}=125\%-150\%$  and  $t_d=5$  s. Additionally, Fig. 10 shows the hysteresis loops of AlSi and AlSi\_N\_HT6, under  $T_{max}=250$  °C,  $K_{TM}=125\%-150\%$  and  $t_d=5$  s. Finally, in Tabs. 4 and 5, a comparison of TMF lifetime and the stress relaxation is made respectively under different testing conditions for AlSi and AlSi\_N\_HT6.

The hysteresis loops of AlSi and AlSi\_N\_HT6 containing the stress versus the mechanical strain and the stress versus the thermal strain at mid-life cycle are depicted in Fig. 8. According to this figure (Fig. 8 (a, b)), the maximum temperature was 250 °C, the thermo-mechanical loading factor was 100%, and the dwell time was 5 s. According to this figure, cyclic softening occurred for AlSi as the stress value decreased during TMF cycles. Notably, at higher temperatures, ageing proceeds more quickly. However, no significant changes were seen in cyclic behavior of AlSi\_N\_HT6 from the hysteresis loops during

TMF testing at 250 °C. Since the plastic strain of base alloy was higher than that of the reinforced specimen due to the higher width of the hysteresis loops, it was inferred that the ductility of the alloy decreased due to nano-clay addition and heat-treating. As also was mentioned in literature [14], the ageing treatment led to the restriction of dislocation motion, which caused a decrease in the ductility of material. Moreover, according to the hysteresis loops of both materials, it was found that the maximum tensile stress was greater than the maximum compressive stress which also was reported in literature [51]. Such a behavior is characteristic of OP-TMF tests.

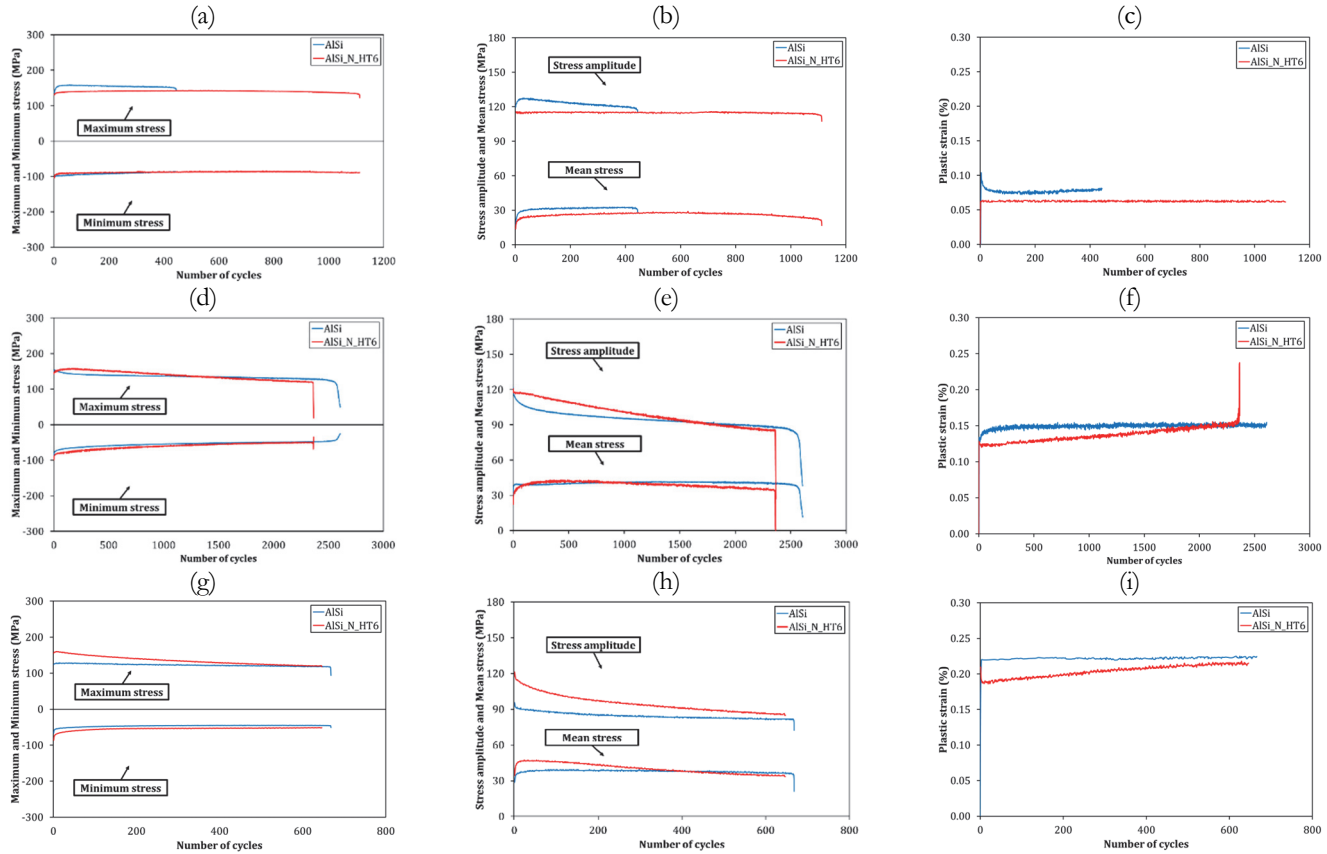


Figure 7: The results for (a)  $\sigma_{max}$  and  $\sigma_{mins}$ , (b)  $\sigma_a$  and  $\sigma_m$ , and (c)  $\epsilon_p$  at  $T_{max}=250$  °C, (d)  $\sigma_{max}$  and  $\sigma_{mins}$ , (e)  $\sigma_a$  and  $\sigma_m$ , and (f)  $\epsilon_p$  at  $T_{max}=300$  °C, (g)  $\sigma_{max}$  and  $\sigma_{mins}$ , (h)  $\sigma_a$  and  $\sigma_m$ , and (i)  $\epsilon_p$  at  $T_{max}=350$  °C, with  $K_{TM}=100\%$ , and  $t_d=5$  s.

The stress-strain hysteresis loops of AISi and AISi\_N\_HT6 at the maximum temperature of 300 °C, with a thermo-mechanical loading factor of 100% and a dwell time of 5 s are illustrated in Fig. 8 (c, d). Since the stress value decreased from the first cycle to the final cycle during TMF testing, it was found that cyclic softening occurred for both reinforced and unreinforced specimens, as also was mentioned before. At the temperature range of 0.5-0.6 of the Al melting point, both diffusion and dislocation creep occur and the material considers to cyclically be softened [5]. Considering Fig. 8 (a-d) shows that as the maximum temperature of TMF testing increased, the maximum stress of both materials decreased and the plastic strain of both materials increased which indicated decreasing the peak stress and increasing the width of hysteresis loops, respectively. The flow stress for corresponding loads decreased by increasing the temperature [11]. It was found that the temperature had more influence than that of the loading on the stress response [11].

The hysteresis loops of stress versus the mechanical strain and the stress versus the thermal strain for TMF testing at the maximum temperature of 350 °C, with the thermo-mechanical loading factor of 100%, and the dwell time of 5 s are depicted in Fig. 8 (e, f). According to this figure, a constant cyclic behavior was observed for AISi during TMF lifetime. In Fig. 7 (h), cyclic softening was seen for AISi\_N\_HT6 as the stress value decreased during fatigue cycles. Such behaviors could also be seen in Fig. 7 (i), which shows the plastic strain of both specimens during fatigue cycles at 350 °C. From this figure, it was observable that the maximum stress decreased for both specimens as the peak stress degraded. It was found that the plastic strain of AISi and AISi\_N\_HT6 increased as the hysteresis loops became wider which shows the softening temperature dependency [11]. At high temperatures, the creation and destruction of the dislocations were increased and the corresponding softening was higher [55].

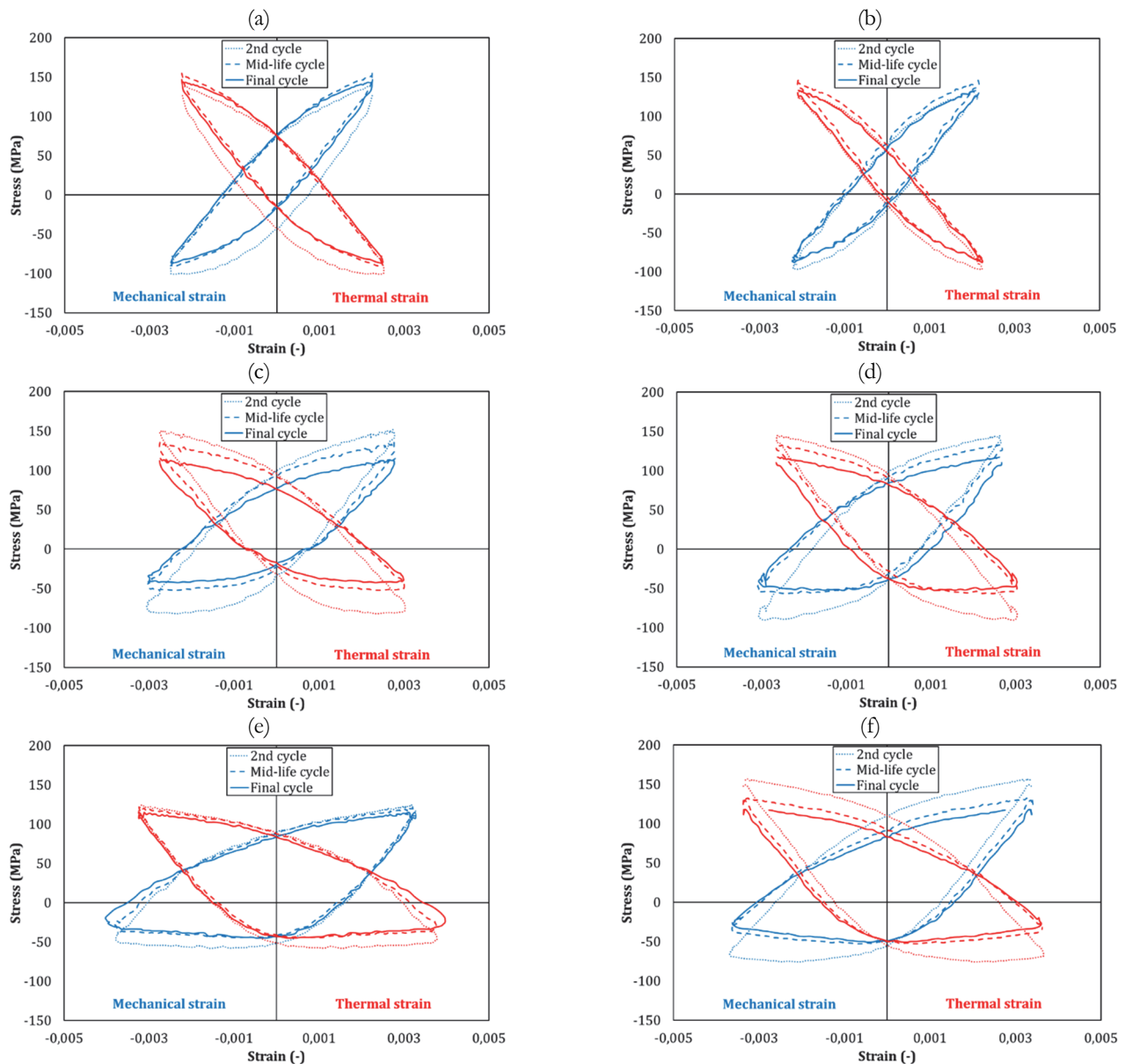


Figure 8: Hysteresis loops of (a) AlSi and (b) AlSi\_N\_HT6 at  $T_{max}=250\text{ }^{\circ}\text{C}$ , (c) AlSi and (d) AlSi\_N\_HT6 at  $T_{max}=300\text{ }^{\circ}\text{C}$ , (e) AlSi and (f) AlSi\_N\_HT6 at  $T_{max}=350\text{ }^{\circ}\text{C}$ , with  $K_{TM}=100\%$  and  $t_d=5\text{ s}$ .

### Thermo-mechanical Loading Factor Effect

The results of maximum and minimum stress, stress amplitude and mean stress, and plastic strain of AlSi and AlSi\_N\_HT6 during fatigue cycles are demonstrated in Fig. 9. It is interesting to note that the maximum temperature was  $250\text{ }^{\circ}\text{C}$ , the thermo-mechanical loading factor was 125%, and the dwell time was 5 s in Fig. 9 (a-c). As seen in this figure the stress amplitude decreased for AlSi during TMF cycles, which means that cyclic softening occurred for the base alloy.

Such behavior could also be seen in Fig. 9 (c) so that the plastic strain increased during the fatigue cycles and after about 600 cycles the plastic strain of AlSi became similar to the plastic strain of AlSi\_N\_HT6. However, no variations were observed for the stress amplitude of AlSi\_N\_HT6 during TMF cycles. Results showed that the reinforcement caused a reduction in the fatigue lifetime by 600 cycles, approximately. Although TMF testing was repeated for the base alloy at these experimental conditions, more tests are needed to be performed for a better investigation of the effect of reinforcements on the TMF lifetime of AlSi alloys. Lower values of stress, higher plastic strain, and lower fatigue lifetime for AlSi\_N\_HT6 indicate that the nano-clay addition and heat-treating increased the ductility and decreased the strength of material. A severe decrement in the TMF lifetime of the reinforced specimen was due to the agglomeration of the nano particles. Comparing

literature [56] and literature [57] with the present work shows that appropriate dispersion of nano particles in the base material had an important role in fatigue behavior. On the other hand, the quality of specimen production and processing is an important issue [58]. Similar conclusions were reached in literature [59] upon which manufacturing parameters such as dispersion of nano particles could have a key role in the fatigue behavior since the interaction between agglomerated reinforcing particles and the matrix could be the fatigue crack nucleation site. Such a problem will be stronger while subjecting the material to low-cycle high-stress fatigue loading [60].

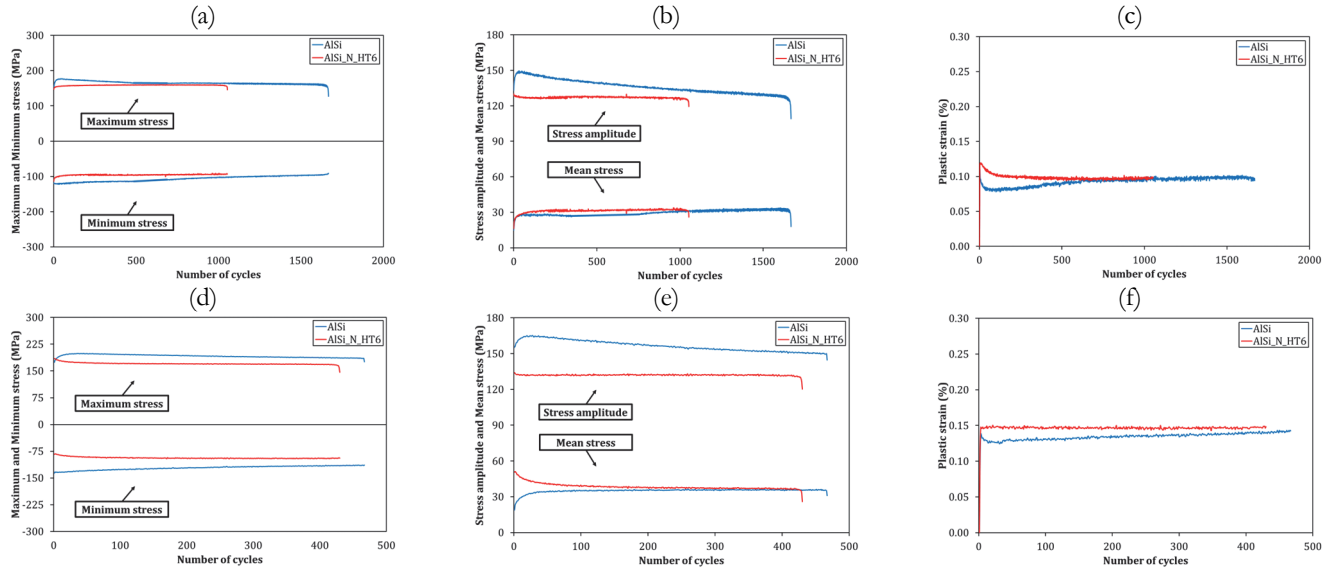


Figure 9: The results for (a)  $\sigma_{max}$  and  $\sigma_{min}$ , (b)  $\sigma_a$  and  $\sigma_m$ , and (c)  $\epsilon_p$  with  $K_{TM}=125\%$ , (d)  $\sigma_{max}$  and  $\sigma_{min}$ , (e)  $\sigma_a$  and  $\sigma_m$ , and (f)  $\epsilon_p$  with  $K_{TM}=150\%$ , with  $T_{max}=250\text{ }^\circ\text{C}$  and  $t_d=5\text{ s}$ .

A similar cyclic behavior was observed in Fig. 9 (d-f) for both materials during fatigue cycles at  $250\text{ }^\circ\text{C}$  with  $K_{TM}=150\%$  and a dwell time of 5 s. According to this figure, cyclic softening occurred for the unreinforced specimen, as the stress decreased and the plastic strain increased during fatigue cycles. Meanwhile, no considerable variation was observed for the stress and plastic strain of the reinforced specimen during TMF cycles. A lack of cyclic softening/hardening for the reinforced material shows the prevailing elastic deformation and arrangement and disarrangement of dislocations [61]. Similar to TMF testing on reinforced and unreinforced specimens under  $T_{max}=250\text{ }^\circ\text{C}$ ,  $K_{TM}=100\%$  and  $t_d=5\text{ s}$ , an initial hardening and then, cyclic softening was seen for fatigue testing on AISi under  $T_{max}=250\text{ }^\circ\text{C}$ ,  $K_{TM}=125\%$  and  $t_d=5\text{ s}$  and  $K_{TM}=150\%$ . As mentioned before, such initial hardening of unreinforced specimen was correlated to the formation of the Al-rich areas [43].

Comparing Fig. 7 (a-c) and Fig. 9 (a-f) representing the TMF testing with  $K_{TM}=100\%$ ,  $125\%$  and  $150\%$ , at the temperature of  $250\text{ }^\circ\text{C}$ , demonstrated that as the thermo-mechanical loading factor increased, the stress amplitude of both specimens also increased. However, such an increase was more for AISi than that of AISi\_N\_HT6. It was also found from such figures that increasing the  $K_{TM}$  led to an increase in the plastic strain of AISi\_N\_HT6 which means that increasing the  $K_{TM}$  increased the ductility of the material.

According to Eqn. (1), higher value of  $K_{TM}$  caused higher values of mechanical strain. At higher values of total strain amplitudes, the stress level increases which was due to more resistance against dislocation slip and plasticity [47].

Fig. 10 (a, b) shows the hysteresis loops of TMF testing under  $T_{max}=250\text{ }^\circ\text{C}$ ,  $K_{TM}=125\%$  and  $t_d=5\text{ s}$  for reinforced and unreinforced specimens. A slight cyclic softening for the base alloy was observed in this figure. However, no meaningful cyclic behavior occurred for the reinforced specimen. Such behavior could also be observed in Fig. 9 (a-c).

Comparing Fig. 10 (a-d) and Fig. 8 (a, b) demonstrated that as the thermo-mechanical loading factor increased, the maximum stress enhanced due to an increase in the mechanical strain amplitude. Besides, no differences were seen for the plastic strain of reinforced and unreinforced specimens since the width of the hysteresis loops (Fig. 10 (a-d) and Fig. 8 (a, b)) are similar to each other.

The hysteresis loops of TMF testing at the maximum temperature of  $250\text{ }^\circ\text{C}$ , with a thermo-mechanical loading factor of  $150\%$  and a dwell time of 5 s is depicted in Fig. 10 (c, d). As mentioned before, increasing the thermo-mechanical loading factor led to an increase in the mechanical strain of material and consequently, the maximum stress of both specimens increased. Comparing Fig. 8 (a, b) and Fig. 10 (a-d) indicates that both AISi alloy and metal-matrix nano-composites had the highest plastic strain under  $T_{max}=250\text{ }^\circ\text{C}$ ,  $K_{TM}=150\%$  and  $t_d=5\text{ s}$ .

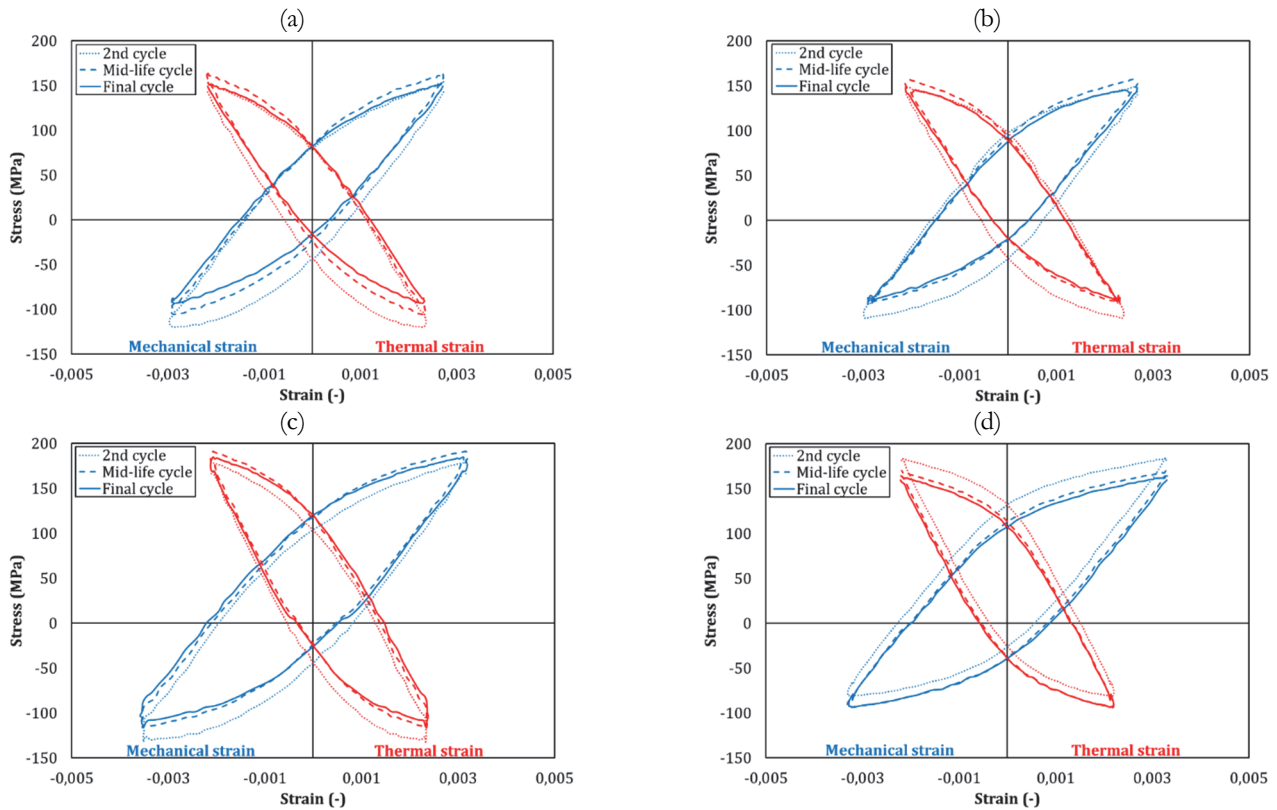


Figure 10: Hysteresis loops of (a) AlSi and (b) AlSi\_N\_HT6 with  $K_{TM}=125\%$ , (c) AlSi and (d) AlSi\_N\_HT6 with  $K_{TM}=150\%$ , with  $T_{max}=250\text{ }^{\circ}\text{C}$  and  $t_d=5\text{ s}$ .

Tab. 4 shows the comparison between results of two different objectives consisting the temperature effect and thermo-mechanical loading factor effect on TMF lifetime of reinforced and unreinforced specimens. It should be noted that in some cases, the TMF tests were repeated due to the huge differences between the fatigue lifetime of reinforced and unreinforced specimens. As seen in this table, while studying the temperature effect, both unreinforced and reinforced specimens had the maximum TMF lifetime under  $T_{max}=300\text{ }^{\circ}\text{C}$ ,  $K_{TM}=100\%$  and  $t_d=5\text{ s}$  which were 2574 and 2359 cycles, respectively. Through investigation of the thermo-mechanical loading factor effect, the maximum fatigue lifetime for unreinforced specimen occurred at the maximum temperature of  $250\text{ }^{\circ}\text{C}$  with  $K_{TM}$  of  $125\%$ , and the dwell time of  $5\text{ s}$ , which was equal to 1659 cycles. Such value for the metal-matrix nano-composites was 1112 cycles, under  $T_{max}=250\text{ }^{\circ}\text{C}$ ,  $K_{TM}=100\%$  and  $t_d=5\text{ s}$ .

Considering all testing conditions showed that AlSi and AlSi\_N\_HT6 had the maximum TMF lifetime under the same testing conditions ( $T_{max}=300\text{ }^{\circ}\text{C}$ ,  $K_{TM}=100\%$  and  $t_d=5\text{ s}$ ) which were equal to 2574 and 2359 cycles, respectively. It means that the optimum temperature for reinforced and unreinforced specimens was  $300\text{ }^{\circ}\text{C}$ . Notably, for the reinforced specimen, as the  $K_{TM}$  increased, the fatigue lifetime decreased.

Stress relaxation is a time-dependent stress reduction in a constant strain value. In other words, in TMF tests, through the dwell time, the stress declines due to stress relaxation as a function of time [62]. Tab. 5 shows the stress relaxation of AlSi and AlSi\_N\_HT6 under TMF testing at the maximum temperatures of  $250\text{ }^{\circ}\text{C}$ ,  $300\text{ }^{\circ}\text{C}$  and  $350\text{ }^{\circ}\text{C}$  with the thermo-mechanical loading factor of  $100\%$  and the dwell time of  $5\text{ s}$  and also at the maximum temperature of  $250\text{ }^{\circ}\text{C}$  with the thermo-mechanical loading factors of  $125\%$  and  $150\%$  and the dwell time of  $5\text{ s}$ , both at mid-life cycle. According to Tab. 5, as the temperature increased, the stress relaxation of both specimens also increased. Comparing the stress relaxation of AlSi and AlSi\_N\_HT6 showed that the reinforcement degraded the stress relaxation of material. However, such decrement was not considerable at the maximum temperature of  $250\text{ }^{\circ}\text{C}$ . As reported in literature [63], the amount of stress relaxation is related to the maximum testing temperature. The stress relaxation through increasing the temperature would increase the mean stress [5]. It is due to decreasing the compressive stress because of the stress relaxation which would enhance the mean stress. Enhancement of the mean stress due to increasing the temperature could also be observed in Figs. 7-9 in which the mean stress increased as the temperature and consequently, the stress relaxation increased (Tab. 5). Lower compressive stress led to higher tensile stress in the next cycle which shows the interdependency of compressive and tensile stress [64].



In this table, it is obvious that increasing the thermo-mechanical loading factor augmented the stress relaxation as the same as the temperature. Although, under TMF testing with  $K_{TM}=125\%$  the stress relaxation declined compared to TMF testing with  $K_{TM}=100\%$ . Increasing the stress relaxation due to the increment of thermo-mechanical loading factor was due to an enhancement in the mechanical strain which led to an increase in the maximum stress. Such observation was aligned with the results reported in literature [64] in which it was pointed out that higher dwell time resulted in higher maximum stress and consequently, higher stress relaxation.

Specimen	$K_{TM}$ (%)	$T_{max}$ (°C)	$t_d$ (s)	TMF lifetime (cycle)
AlSi	100	250	5	401
AlSi	100	250 (repeated)	5	443
AlSi	100	300	5	2574
AlSi	100	350	5	667
AlSi_N_HT6	100	250	5	1112
AlSi_N_HT6	100	300	5	2359
AlSi_N_HT6	100	350	5	152
AlSi_N_HT6	100	350 (repeated)	5	646
AlSi	125	250	5	723
AlSi	125 (repeated)	250	5	1659
AlSi	150	250	5	466
AlSi_N_HT6	125	250	5	1051
AlSi_N_HT6	150	250	5	428

Table 4: Comparison of TMF lifetime under different testing conditions.

#### Fractography on fractured surface of samples

The SEM images of fatigue fracture surfaces of AlSi and AlSi\_N\_HT6 under testing conditions of  $K_{TM}=100\%$ ,  $t_d=5$  s at 250 °C and 350 °C, are illustrated in Fig. 11. In this figure, different marks such as cleavage, quasi-cleavage, tear-ridge, and micro-crack were observed for AlSi which indicated the brittle fracture of specimens through the fatigue testing [65]. It is interesting to note that in some cases, tear-ridge shows the local ductility of the material [66]. Moreover, tear-ridges were the sign of the transition region from slow fatigue to fast [66]. Additionally, such tear-ridges indicate high ductility against plastic deformation [67].

Specimen	$K_{TM}$ (%)	$T_{max}$ (°C)	$t_d$ (s)	Stress relaxation (MPa)
AlSi	100	250	5	9
AlSi	100	300	5	13
AlSi	100	350	5	14
AlSi_N_HT6	100	250	5	8
AlSi_N_HT6	100	300	5	9
AlSi_N_HT6	100	350	5	10
AlSi	125	250	5	11
AlSi	150	250	5	23
AlSi_N_HT6	125	250	5	5
AlSi_N_HT6	150	250	5	12

Table 5: Stress relaxation of AlSi and AlSi\_N\_HT6 under different TMF testing conditions.

The Al alloys mainly had a ductile fracture mechanism and the cleavage fracture appears only under special conditions [68]. Although according to Fig. 11, increasing the temperature did not change the fracture mechanism and it was still brittle [69],

it was seen that as the temperature increased, the cleavage also increased in the AlSi fracture surface. It was also inferred from Fig. 11 (b, d) that increasing the temperature from 250 °C to 350 °C caused AlSi<sub>N</sub>\_HT6 fracture surface to be changed from cleavage to the quasi-cleavage near to dimple. However, the reinforced specimen also had a brittle fracture due to the same marks as AlSi. The fracture surface with dimple-shaped morphologies was representative of a finer microstructure and the spheroidized Si particles [70].

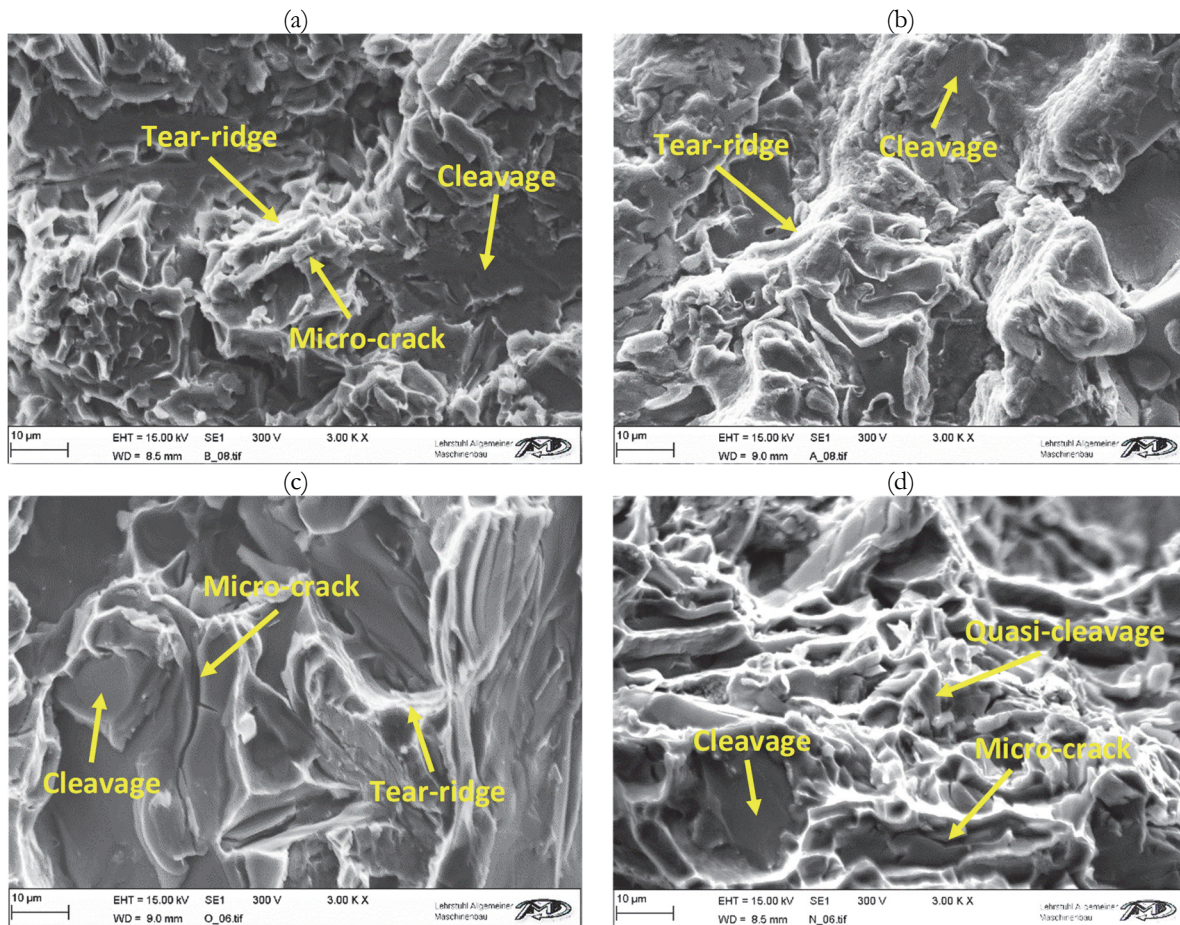


Figure 11: SEM images of fracture surface of (a) AlSi at  $T_{max}=250$  °C, (b) AlSi at  $T_{max}=350$  °C, (c) AlSi<sub>N</sub>\_HT6 at  $T_{max}=250$  °C, and (d) AlSi<sub>N</sub>\_HT6 at  $T_{max}=350$  °C, after TMF testing with  $K_{TM}=100\%$  and  $t_d=5$  s.

Fig. 12 shows the fracture surface of unreinforced specimen and reinforced specimen with nano-clay particles and heat treatment, under fatigue testing at the maximum temperature of 250 °C with  $K_{TM}=150\%$  and  $t_d=5$  s. It could be observed that the  $K_{TM}$  had no effect on the fracture type and both specimens had still brittle fractures. However, the fatigue lifetime was affected by the  $K_{TM}$ . According to this figure, as the Al alloy was reinforced by nano particles and heat treatment, the plate-like morphologies appeared on the fracture surface.

In Figs. 11 and 12, the intergranular mixed with the transgranular crack growth was observed in fracture surfaces. As seen, the "rocky candy" pattern shows the intergranular cracking [71] and the "plate-like" features are representative of transgranular cracking [72]. Indeed, the inherent grains structures play an important role in fatigue crack nucleation and also fatigue crack growth behavior [73]. Intergranular fracture is an uncommon phenomenon in fatigue loading of ductile metals which occurs in special conditions and controls by the temperature and strain rate [74]. The hard intermetallics in grain boundary cause the stress concentration which led to intergranular fracture [71]. The adjacent grains with soft orientation let the slip bands pass along the grain boundaries and get into the soft grains due to their easy dislocation activities [75] before the transgranular crack growth. Such grains would strongly reduce the crack propagation resistance of the material [76]. The flat cracks were grown perpendicular to the loading direction with transgranular cracking in recrystallized grains and also intergranular and transgranular fracture in subgrains [73]. The subgrains with low-angle grain boundaries simplify passing the slip bands through nearby grains for ongoing transgranular cracking. The high-strength subgrains with low plastic deformation apply the plastic deformation and stress to the adjacent grains, which results in transgranular cracking.

Such transgranular crack propagations within subgrains reduce the crack growth rate and enhance the fatigue lifetime [77]. Materials with more subgrains near the surface would have a lower crack growth rate and longer fatigue lifetime [73]. The plastic deformation from the slip bands initiated from the surface recrystallized grains can nucleate the surficial micro-cracks which would propagate as transgranular and intergranular cracking [73].

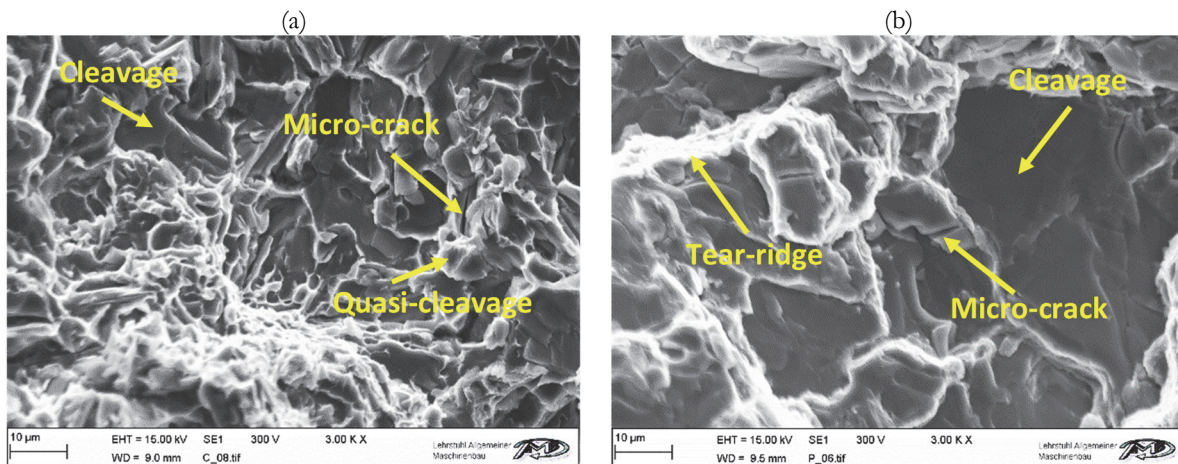


Figure 12: SEM images of the fracture surface in (a) AlSi and (b) AlSi\_N\_HT6 under TMF testing at  $T_{max}=250$  °C with  $K_{TM}=150\%$  and  $t_d=5$  s

Fig. 13 represents the EDS mapping of fracture surface of reinforced and unreinforced specimens at the maximum temperature of 250 °C and 350 °C under TMF testing with  $K_{TM}=100\%$  and  $t_d=5$  s. In this figure, the Al matrix, Si-rich, Mg-rich, Mn-rich, and Ni-rich phases were observed on the fracture surface of base alloy and reinforced sample. Some small micro-cracks could also be seen in the Al matrix and intermetallic phases.

Such fatigue micro-cracks were propagated in different directions due to various microstructures of the material which led to the transfer of the micro-cracks between planes [78]. As seen in the EDS mapping of the fatigue fracture surface, the micro-cracks mainly were detected in the Si-rich phase [70]. Furthermore, thermal cycles would cause the Si particle expansion and also plasticity around the Al matrix, which accelerate the deformation of composite [10]. Through TMF testing, the Si particles rupture by main cracks and the other hard particles are induced by fatigue [36]. The crack initiation mainly occurs from Si particles [79]. While plastic deformation occurs in the matrix, the Si particles could prevent the sliding movement and material deformation due to their lower deformation capability [51]. The matrix near Si particles easily deformed since the material cooled down from high temperatures, which caused a generation of dislocation [51]. The main reason for the dislocation arrangement is different coefficients of thermal expansion between the matrix and Si phase [80]. The severe plastic deformation around Si particles is due to low active energy to overcome the interface between Si phase and matrix [81]. The large-size Si particles act as a barrier for dislocation which led to stress concentration [43]. As these particles could not accommodate plastic deformation, the crack nucleation became easier which led to the decohesion of Si particles [43]. The Si particles had high elasticity and low plasticity which are more sensitive to the stress and strain flow to the Al matrix while subjected to cyclic loading [45]. It was also mentioned in literature [70] that the fatigue cracks mainly initiated from pores [82] and propagated through the plate-like eutectic Si particles. It was due to stress concentration which was induced around the plate-like Si particles and caused the plastic deformation during fatigue cycles and were more susceptible to crack propagation [70]. The plate-like and needle-shaped Si particles were prone to fracture compared to fine and well-dispersed Si particles [75]. As pointed out in literature [83], the fatigue propagation rate in metals is mainly controlled by the microstructure and plastic zone size. Under TMF loading, the fracture of intermetallics would cause to initiate the micro-cracks [84]. In addition, the cracks mainly propagated through the brittle phase [84]. Increasing the temperature could cause the micro-cracks to be disappeared from the fracture surface [69]. It was due to increasing the plastic strain which promotes the ductility of material.

Although the fracture surfaces of both AlSi and AlSi\_N\_HT6 were characterized using SEM images, using transmission electron microscopy (TEM) is strongly needed for accurate evaluation and will be performed in the next work.

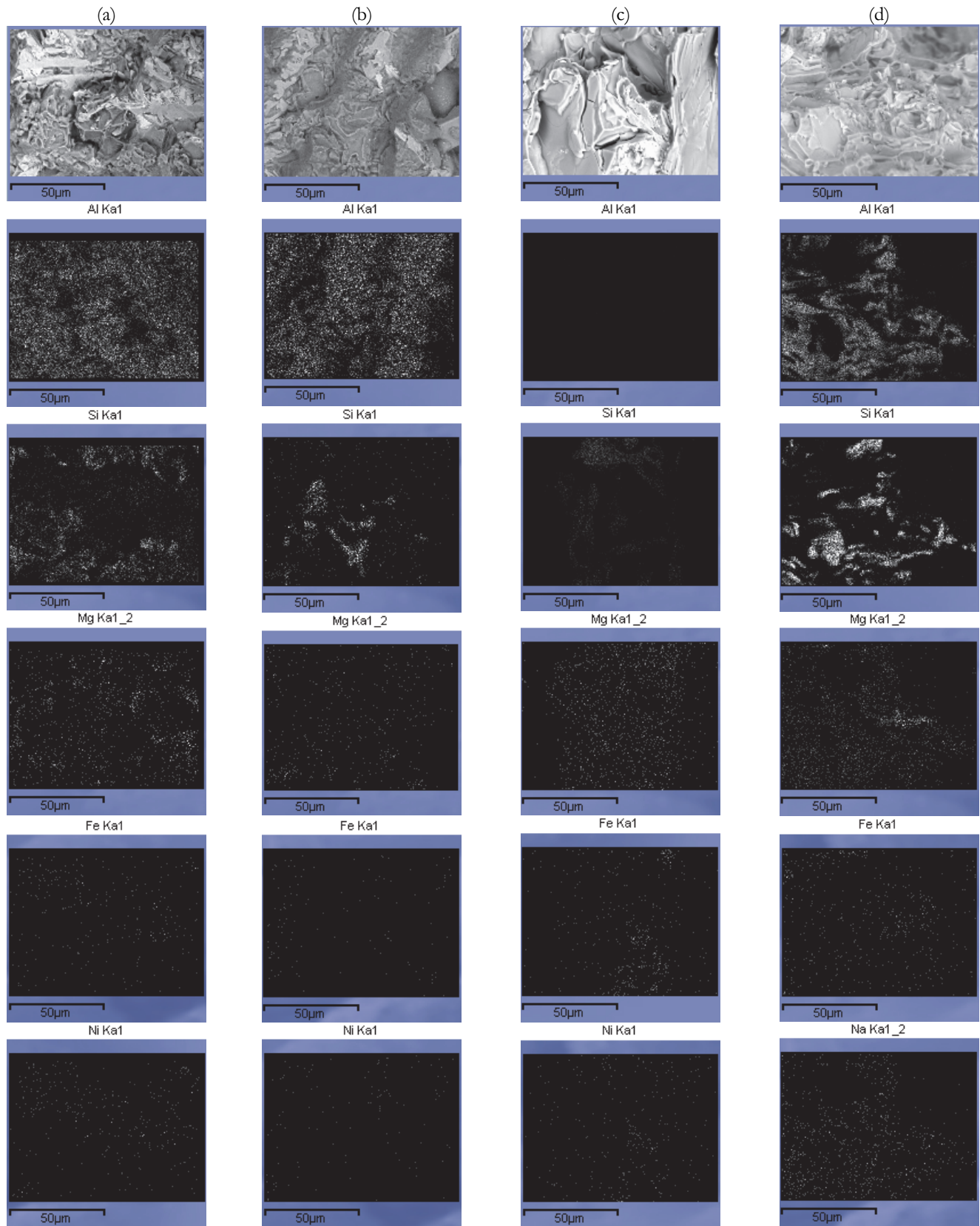


Figure 13: EDS mapping on the fracture surface of (a) AlSi at  $T_{max}=250$  °C, (b) AlSi at  $T_{max}=350$  °C, (c) AlSi\_N-HT6 at  $T_{max}=250$  °C, and (d) AlSi\_N-HT6 at  $T_{max}=350$  °C, under TMF testing with  $K_{TM}=100\%$  and  $t_d=5$  s.



## CONCLUSIONS

In the presented article, the OP-TMF behavior of the piston AlSi alloy and the Al-matrix nano-composites reinforced by nano-clay particles and heat-treating was explored. Obtained experimental results are as follows:

- The reinforcement led to longer fatigue lifetimes (668 cycles higher, more than 2 times higher), when the maximum temperature was 250 °C. The root cause was the changes in the material microstructure by nano particles and heat-treating. The plastic strain history was 15% lower in the Al alloy compared to the nano-composites; however, it was not generally significant.
- When the maximum temperature increased to 300 °C, after about 1500 cycles (almost half of the fatigue lifetime), the stress value become similar in both samples of the Al alloy and the nano-composites. This issue was due to the over-ageing phenomenon at 300 °C in the material. Generally, higher maximum temperatures could not affect the fatigue lifetime, when there was a reinforcement.
- When the maximum temperature was 250 °C and the thermo-mechanical loading factor changed from 100 to 150%, the stress and the plastic strain increased as expected in the material. However, this enhancement was more in AlSi alloy compared to the nano-composites. This difference issue was due to the higher resistance of the nano-composites against the dislocation slip.
- The fracture behavior of both studied materials was brittle due to cleavage and quasi-cleavage marks on the fracture surface of the samples. Higher temperatures led to irreversible loss in the resistance to deformation of the materials and different thermo-mechanical loading factors had no significant effects on the fracture behavior. Additionally, both materials exhibited intergranular mixed with transgranular fracture mode.

## ACKNOWLEDGMENT

This research is financed by the Austrian Agency for International Cooperation in Education and Research (OeAD) and the Ministry of Science, Research and Technology of Iran (MSRT), and also Kharazmi University in Iran, through the IMPULSE funding program. In addition, authors tend to thank the Motorsazi Pooya Neyestanak (MPN) Company, in Iran for casting and raw materials.

## REFERENCES

- [1] Azadi, M., Bahmanabadi, H., Gruen, F., Winter, G., Seisenbacher, B. (2022). Cyclic hardening/softening experimental data in nano-clay-composite and aluminum alloy under high-temperature strain-controlled loading, *Exp. Results.*, 3, pp. e6, DOI: 10.1017/exp.2021.32.
- [2] Minichmayr, R., Riedler, M., Winter, G., Leitner, H., Eichlseder, W. (2008). Thermo-mechanical fatigue life assessment of aluminium components using the damage rate model of Sehitoglu, *Int. Fatigue.*, 30, pp. 298–304. DOI: 10.1016/j.ijfatigue.2007.01.054.
- [3] Neu, R.W., Sehitoglu, H. (1989). Thermomechanical fatigue, oxidation, and Creep Part II. Life prediction, *Metall. Trans., A*, 20, pp. 1769–1783. DOI: 10.1007/BF02663208.
- [4] Azadi, M., Farrahi, G.H., Winter, G., Huter, P., Eichlseder, W. (2015). Damage prediction for un-coated and coated aluminum alloys under thermal and mechanical fatigue loadings based on a modified plastic strain energy approach, *Mater. Des.*, 66, pp. 587–595. DOI: 10.1016/j.matdes.2014.04.022.
- [5] Azadi, M., Ghodrati, M., Farrahi, G.H. (2014). Experimental and numerical evaluations of stress relaxation in A356 aluminium alloy subjected to out-of-phase thermomechanical cyclic loadings, *Mater. at High Temp.*, 31, pp. 204–210. DOI: 10.1179/1878641314Y.0000000015.
- [6] Sasaki, K., Takahashi, T. (2006). Low cycle thermal fatigue and microstructural change of AC2B-T6 aluminum alloy, *Int. J. Fatigue.*, 28, pp. 203–210. DOI: 10.1016/j.ijfatigue.2005.06.025.
- [7] Zhang, S., Wang, Z., Han, Y., Zheng, Y., Zhang, D. (2020). Experimental and theoretical studies on thermo-mechanical fatigue test for aluminium cast alloy, *Fatigue Fract. Eng. Mater. Struct.*, 43, pp. 110–118. DOI: 10.1111/ffe.13076.
- [8] Li, Z., Li, J., Chen, Z., Guo, J., Zhu, Y., Luo, Y. (2021). Experimental and computational study on thermo-mechanical fatigue life of aluminium alloy piston, *Fatigue Fract. Eng. Mater. Struct.*, 44, pp. 141–155. DOI: 10.1111/ffe.13342.



- [9] Azadi, M., Shirazabad, M.M. (2013). Heat treatment effect on thermo-mechanical fatigue and low cycle fatigue behaviors of A356.0 aluminum alloy, *Mater. Des.*, 45, pp. 279–285. DOI: 10.1016/j.matdes.2012.08.066.
- [10] Wang, M., Pang, J.C., Zhang, M.X., Liu, H.Q., Li, S.X., Zhang, Z.F. (2018). Thermo-mechanical fatigue behavior and life prediction of the Al-Si piston alloy, *Mater. Sci. & Eng. A.*, 715, pp. 62–72. DOI: 10.1016/j.msea.2017.12.099.
- [11] Natesan, E., Meyer, K.A., Eriksson, S., Ahlström, J., Persson, C. (2020). Effects of dwell time on the deformation and fatigue behaviour of A356-T7 cast aluminium alloys used in high specific power IC engine cylinder heads, *Materials.*, 13(12), pp. 2727. DOI: 10.3390/ma13122727.
- [12] Merhy, E., Rémy, L., Maitournam, H., Augustins, L. (2013). Crack growth characterisation of A356-T7 aluminum alloy under thermo-mechanical fatigue loading, *Eng. Fract. Mech.*, 110, pp. 99–112. DOI: 10.1016/j.engfracmech.2013.03.019.
- [13] Azadi, M., Farrahi, G.H., Winter, G., Eichlleder, W. (2013). Experimental fatigue lifetime of coated and uncoated aluminum alloy under isothermal and thermo-mechanical loadings, *Ceram Int.*, 39, pp. 9099–9107. DOI: 10.1016/j.ceramint.2013.05.006.
- [14] Azadi, M. (2017). Cyclic thermo-mechanical stress, strain and continuum damage behaviors in light alloys during fatigue lifetime considering heat treatment effect, *Int. J. Fatigue.*, 99, pp. 303–314. DOI: 10.1016/j.ijfatigue.2016.12.001.
- [15] Fischer, C., Schweizer, C. (2021). Experimental investigation of the damage characteristics of two cast aluminium alloys Part I – Temperature dependent low cycle and thermomechanical fatigue behavior, *Int. J. Fatigue.*, 152, pp. 106359. DOI: 10.1016/j.ijfatigue.2021.106359.
- [16] Beck, T., Lang, K.-H., Löh, D. (2001). Thermal–mechanical fatigue behaviour of cast aluminium alloys for cylinder heads reinforced with 15 vol.% discontinuous Al<sub>2</sub>O<sub>3</sub> (Saffil) fibers. *Mater. Sci. & Eng. A.*, 319–321, 662–666. DOI: 10.1016/S0921-5093(00)02022-0.
- [17] Khisheh, S., Azadi, M., Hendoabadi, V.Z., Parast, M.S.A., Winter, G., Seisenbacher, B., Gruen, F., Khalili, K. (2022). Influence of T6 heat-treating and over-ageing on out-of-phase thermo-mechanical fatigue behaviors of Al-Si-Cu alloy, *Mater. Today Commun.*, 33, pp. 104803. DOI: 10.1016/j.mtcomm.2022.104803.
- [18] Azadi, M. (2013). Effects of strain rate and mean strain on cyclic behavior of aluminum alloys under isothermal and thermo-mechanical fatigue loadings, *Int. J. Fatigue.*, 47, pp. 148–153. DOI: 10.1016/j.ijfatigue.2012.08.005.
- [19] Wang, M., Pang, J.C., Liu, H.Q., Li, S.X., Zhang, M.X., Zhang, Z.F. (2020). Effect of constraint factor on the thermo-mechanical fatigue behavior of an Al-Si eutectic alloy, *Mater. Sci. & Eng. A.*, 783, pp. 139279. DOI: 10.1016/j.msea.2020.139279.
- [20] Bose-Filho, W.W., de Freitas, E.R., da Silva, V.F., Milan, M.T., Spinelli, D. (2007). Al-Si cast alloys under isothermal and thermomechanical fatigue conditions, *Int. J. Fatigue.*, 29, pp. 1846–1854. DOI: 10.1016/j.ijfatigue.2007.01.006.
- [21] Wagner, M., Mösenbacher, A., Eiber, M., Hoyer, M., Riva, M., Christ, H.J. (2019). Thermomechanical fatigue of lost foam cast Al–Si cylinder heads—assessment of crack origin based on the evaluation of pore distribution, *Metals*, 9(8), pp. 821. DOI: 10.3390/met9080821.
- [22] Takahashi, T., Sasaki, K. (2010). Low cycle thermal fatigue of aluminum alloy cylinder head in consideration of changing metrology microstructure, *Procedia Eng.*, 2, pp. 767–776. DOI: 10.1016/j.proeng.2010.03.083.
- [23] Grieb, M.B., Christ, H.J., Plege, B. (2010). Thermomechanical fatigue of cast aluminium alloys for cylinder head application experimental characterization and life prediction, *Procedia Eng.*, 2, pp. 1767–1776. DOI: 10.1016/j.proeng.2010.03.190.
- [24] Zhu, M., Jian, Z., Yang, G., Zhou, Y. (2012). Effects of T6 heat treatment on the microstructure, tensile properties, and fracture behavior of the modified A356 alloys, *Materials & Design.*, 36, pp. 243–249. DOI: 10.1016/j.matdes.2011.11.018.
- [25] Ogris, E., Wahlen, A., Lüchinger, H., Uggowitzer, P.J. (2002). On the silicon spheroidization in Al-Si alloys, *J. Light Met.* 2, pp. 263–269. DOI: 10.1016/S1471-5317(03)00010-5.
- [26] Bahmanabadi, H., Azadi, M. (2022). Sensitivity Analysis of Solutioning Time, Ageing Temperature, and Clay Nano-Particles Addition on Hardness of Piston Aluminum-Silicon Alloy using Regression Method, *J. Metall. & Mater. Eng.*, 33, pp. 67–94. DOI: 10.22067/JMME.2022.75681.1044.
- [27] Azadi, M., Bahmanabadi, H., Gruen, F., Winter, G. (2020). Evaluation of tensile and low-cycle fatigue properties at elevated temperatures in piston aluminum-silicon alloys with and without nano-clay-particles and heat treatment, *Mater. Sci. & Eng. A.*, 788, pp. 139497. DOI: 10.1016/j.msea.2020.139497.
- [28] Wang, M., Pang, J.C., Liu, H.Q., Li, S.X., Zhang, Z.F. (2019). Influence of microstructures on the tensile and low-cycle fatigue damage behaviors of cast Al12Si4Cu3NiMg alloy, *Mater. Sci. & Eng. A.*, 759, pp. 797–803. DOI: 10.1016/j.msea.2019.05.016.



- [29] Canyook, R., Utakrut, R., Wongnichakorn, C., Fakpan, K., Kongiang, S. (2018). The effects of heat treatment on microstructure and mechanical properties of rheocasting ADC12 aluminum alloy, *Mater. Today Proceed.*, 5(3), pp. 9476–9482. DOI: 10.1016/j.matpr.2017.10.127.
- [30] Tonelli, L., Refat, M., Toschi, S., Ahmed, M.M.Z., Ahmed, E., Morri, A., El-Mahallawi, I., Ceschini, L. (2019). Production of AlSi12CuNiMg/Al<sub>2</sub>O<sub>3</sub> Micro/Nanodispersed Surface Composites Using Friction Stir Processing for Automotive Applications, Germany, Springer International Publishing, DOI: 10.1007/978-3-030-05752-7\_22.
- [31] Chen, C.-L., Richter, A., Thomson, R.C. (2009). Mechanical properties of intermetallic phases in multi-component Al–Si alloys using nanoindentation, *Intermetallics*, 17, pp. 634–641. DOI: 10.1016/j.intermet.2009.02.003.
- [32] Asghar, Z., Requena, G., Degischer, H.P., Cloetens, P. (2009). Three-dimensional study of Ni aluminides in an AlSi12 alloy by means of light optical and synchrotron microtomography, *Acta Mater.*, 57, pp. 4125–4132. DOI: 10.1016/j.actamat.2009.05.010.
- [33] Jeong, C.-Y. (2012). Effect of Alloying Elements on High Temperature Mechanical Properties for Piston Alloy, *Mater. Trans.*, 53, pp. 234–239. DOI: 10.2320/matertrans.M2011259.
- [34] ISO 12111. (2011). Metallic materials, Fatigue testing, Strain-controlled thermomechanical fatigue testing method.
- [35] Wu, X., Quan, G., MacNeil, R., Zhang, Z., Liu, X., Sloss, C. (2015). Thermomechanical Fatigue of Ductile Cast Iron and Its Life Prediction, *Metall. & Mater. Trans. A.*, 46, pp. 2530–2543. DOI: 10.1007/s11661-015-2873-9.
- [36] Huter, P., Oberfrank, S., Grün, F., Stauder, B. (2016). Thermo-mechanical fatigue influence of copper and silicon on hypo-eutectic Al–Si–Cu and Al–Si–Mg cast alloys used in cylinder heads, *Int. J. Fatigue.*, 88, pp. 142–155. DOI: 10.1016/j.ijfatigue.2016.02.017.
- [37] Liu, H., Pang, J., Wang, M., Li, S., Zhang, Z. (2018). High-Cycle Fatigue Behavior and Damage Mechanism of Multiphase Al–Si Piston Alloy at Room and Elevated Temperatures, *Adv. Eng. Mater.*, 20, pp. 1700972. DOI: 10.1002/adem.201700972.
- [38] Compeau, D.R., Higgins, C.A. (1995). ASTM E2368-10, Standard Practice for Strain Controlled Thermomechanical Fatigue Testing. *MIS Quarterly*, 19, pp. 189–211.
- [39] Haehner, P., Affeldt, E., Beck, T., Klingelhoefter, H., Loveday, M., Rinaldi, C. (2006). Validated code-of-practice for strain controlled thermo-mechanical fatigue testing, ECRreport EUR 22281 EN. Institute for Energy, Petten.
- [40] Wang, M., Pang, J.C., Li, S.X., Zhang, Z.F. (2017). Low-cycle fatigue properties and life prediction of Al–Si piston alloy at elevated temperature, *Mater. Sci. & Eng. A.*, 704, pp. 480–492. DOI: 10.1016/j.msea.2017.08.014.
- [41] Zhang, Q., Zuo, Z., Liu, J. (2013). High-temperature low-cycle fatigue behaviour of a cast Al–12Si–CuNiMg alloy, *Fatigue Fract. Eng. Mater. Struct.*, 36, pp. 623–630. DOI: 10.1111/ffe.12029.
- [42] Magee, A.C., Ladani, L. (2013). Temperature dependency of mechanical behavior and strain rate sensitivity of an Al–Mg alloy with bimodal grain size, *Mater. Sci. & Eng. A.*, 582, pp. 276–283. DOI: 10.1016/j.msea.2013.06.016.
- [43] Li, W., Chen, H., Liang, Z., Chen, J. (2021). Effects of SiC orientations and particle sizes on the low cycle fatigue properties of SiCp/A356 composite, *Int. J. Fatigue.*, 152, pp. 106420. DOI: 10.1016/j.ijfatigue.2021.106420.
- [44] Perng, C.-C., Hwang, J.-R., Doong, J.-L. (1993). Elevated-temperature, low-cycle fatigue behaviour of an Al<sub>2</sub>O<sub>3</sub>p/6061-T6 aluminium matrix composite, *Compos. Sci. Technol.*, 49, pp. 225–236. DOI: 10.1016/0266-3538(93)90105-P.
- [45] Cai, C., Geng, H., Cui, Q., Wang, S., Zhang, Z. (2018). Low cycle fatigue behavior of AlSi10Mg(Cu) alloy at high temperature, *Mater. Charact.*, 145, pp. 594–605. DOI: 10.1016/j.matchar.2018.09.023.
- [46] Leng, L., Zhang, Z.J., Duan, Q.Q., Zhang, P., Zhang, Z.F. (2018). Improving the fatigue strength of 7075 alloy through aging, *Mater. Sci. & Eng. A.*, 738, pp. 24–30. DOI: 10.1016/j.msea.2018.09.047.
- [47] Sajadifar, S. V., Scharifi, E., Wegener, T., Krochmal, M., Lotz, S., Steinhoff, K., Niendorf, T. (2022). On the low-cycle fatigue behavior of thermo-mechanically processed high-strength aluminum alloys, *Int. J. Fatigue.*, 156, pp. 106676. DOI: 10.1016/j.ijfatigue.2021.106676.
- [48] Winter, L., Hockauf, K., Lampke, T. (2018). Temperature and particle size influence on the high cycle fatigue behavior of the SiC reinforced 2124 aluminum alloy, *Metals*, 8(1), pp. 43. DOI: 10.3390/met8010043.
- [49] Dowling, N.E. (2013). *Mechanical Behavior of Materials Engineering Methods for Deformation, Fracture, and Fatigue*. Pearson, Virginia.
- [50] Tabibian, S., Charkaluk, E., Constantinescu, A., Guillemot, G., Szymtka, F. (2015). Influence of process-induced microstructure on hardness of two Al–Si alloys, *Mater. Sci. & Eng. A.*, 646, pp. 190–200. DOI: 10.1016/j.msea.2015.08.051.
- [51] Li, W., Chen, H., Zuo, L., Chen, J., Xu, D., He, J., Li, C., Peng, Z., Ren, Y., Zhang, S. De (2015). Thermomechanical Fatigue Behavior of Spray-Deposited SiCp/Al–Si Composite Applied in the High-Speed Railway Brake Disc, *Int. J. Photoenergy*, 2020, pp. 6150794. DOI: 10.1155/2020/6150794.



- [52] Beck, T., Löhe, D., Luft, J., Henne, I. (2007). Damage mechanisms of cast Al-Si-Mg alloys under superimposed thermal-mechanical fatigue and high-cycle fatigue loading, *Mater. Sci. & Eng. A.*, 468–470, pp. 184–192. DOI: 10.1016/j.msea.2006.05.177.
- [53] Estey, C.M., Cockcroft, S.L., Maijer, D.M., Hermesmann, C. (2004). Constitutive behaviour of A356 during the quenching operation, *Mater. Sci. & Eng. A.*, 383, pp. 245–251. DOI: 10.1016/j.msea.2004.06.004.
- [54] Zhang, X., Ahmmed, K., Wang, M., Hu, H. (2012). Influence of aging temperatures and times on mechanical properties of vacuum high pressure die cast aluminum alloy a356, *Adv. Mat. Res.*, 445, pp. 277–282. DOI: 10.4028/www.scientific.net/AMR.445.277.
- [55] Zhou, M., Lin, Y.C., Deng, J., Jiang, Y.Q. (2014). Hot tensile deformation behaviors and constitutive model of an Al-Zn-Mg-Cu alloy, *Mater. Des.*, 59, pp. 141–150. DOI: 10.1016/j.matdes.2014.02.052.
- [56] Srivatsan, T.S., Godbole, C., Paramsothy, M., Gupta, M. (2012). The role of aluminum oxide particulate reinforcements on cyclic fatigue and final fracture behavior of a novel magnesium alloy, *Mater. Sci. & Eng. A.*, 532, pp. 196–211. DOI: 10.1016/j.msea.2011.10.081.
- [57] Raju, P.R.M., Rajesh, S., Raju, K.S.R., Raju, V.R. (2017). Evaluation of Fatigue Life of Al<sub>2</sub>O<sub>3</sub>/Al<sub>2</sub>O<sub>3</sub> Particulate Nano Composite Fabricated Using Stir Casting Technique, *Mater. Today Proc.*, 4, pp. 3188–3196. DOI: 10.1016/j.matpr.2017.02.204.
- [58] Malaki, M., Xu, W., Kasar, A.K., Menezes, P.L., Dieringa, H., Varma, R.S., Gupta, M. (2019). Advanced metal matrix nanocomposites, *Metals*, 9(3), pp. 330. DOI: 10.3390/met9030330.
- [59] Nafar Dastgerdi, J., Marquis, G., Sankaranarayanan, S., Gupta, M. (2016). Fatigue crack growth behavior of amorphous particulate reinforced composites, *Compos. Struct.*, 153, pp. 782–790. DOI: 10.1016/j.compstruct.2016.06.071.
- [60] Malaki, M., Tehrani, A.F., Niroumand, B. (2020). Fatigue behavior of metal matrix nanocomposites, *Ceram Int.*, 46, pp. 23326–23336. DOI: 10.1016/j.ceramint.2020.06.246.
- [61] Picak, S., Wegener, T., Sajadifar, S. V., Sobrero, C., Richter, J., Kim, H., Niendorf, T., Karaman, I. (2021). On the low cycle fatigue response of CoCrNiFeMn high entropy alloy with ultra-fine grain structure, *Acta Mater.*, 205, pp. 116540. DOI: 10.1016/j.actamat.2020.116540.
- [62] Ashter, S.A. Characterization, In: *Thermoforming of Single and Multilayer Laminates*, London, Elsevier Publishing, pp. 147–192. (2014). DOI: 10.1016/B978-1-4557-3172-5.00007-4.
- [63] Oh, Y.-J., Yang, W.-J., Jung, J.-G., Choi, W.-D. (2012). Thermomechanical fatigue behavior and lifetime prediction of niobium-bearing ferritic stainless steels, *Int. J. Fatigue.*, 40, pp. 36–42. DOI: 10.1016/j.ijfatigue.2012.01.013.
- [64] Ghodrati, S., Riemsdijk, T.A.C., Kestens, L.A.I., Petrov, R.H., Janssen, M., Sietsma, J. (2013). Effects of Holding Time on Thermomechanical Fatigue Properties of Compacted Graphite Iron Through Tests with Notched Specimens, *Metall. & Mater. Trans. A.*, 44, pp. 2121–2130. DOI: 10.1007/s11661-012-1320-4.
- [65] Fan, K.L., Liu, X.S., He, G.Q., Chen, H. (2015). Elevated temperature low cycle fatigue of a gravity casting Al-Si-Cu alloy used for engine cylinder heads, *Mater. Sci. & Eng. A.*, 632, pp. 127–136. DOI: 10.1016/j.msea.2015.02.069.
- [66] Contreras, A., Vogt, R.G., Oliveira, D.M., Schoenung, J.M., Gibeling, J.C. (2021). Low Cycle Fatigue of an Ultrafine Grained AA5083 Aluminum Alloy Composite Produced by Cryomilling, *Metall. Mater. Trans. A Phys. Metall. Mater. Sci.*, 52, pp. 975–984. DOI: 10.1007/s11661-020-06129-w.
- [67] Srivatsan, T.S., Al-Hajri, M., Hannon, W., Vasudevan, V.K. (2004). The strain amplitude-controlled cyclic fatigue, deformation and fracture behavior of 7034 aluminum alloy reinforced with silicon carbide particulates, *Mater. Sci. & Eng. A.*, 379, pp. 181–196. DOI: 10.1016/j.msea.2004.01.039.
- [68] Committee, A.S.M.H. *Fractography*, (1987). DOI: 10.31399/asm.hb.v12.9781627081818.
- [69] Liu, J., Zhang, Q., Zuo, Z., Xiong, Y., Ren, F., Volinsky, A.A. (2013). Microstructure evolution of Al-12Si-CuNiMg alloy under high temperature low cycle fatigue, *Mater. Sci. & Eng. A.*, 574, pp. 186–190. DOI: 10.1016/j.msea.2013.03.027.
- [70] Fan, K.L., Liu, X.S., He, G.Q., Cheng, H., Lv, S.Q. (2015). Strain Ratio Effects on Low-Cycle Fatigue Behavior of Gravity Cast Al-Si-Cu Alloys, *J. Mater. Eng. Perform.*, 24, pp. 3942–3950. DOI: 10.1007/s11665-015-1656-1.
- [71] Li, Y., Qiu, S., Zhu, Z., Han, D., Chen, J., Chen, H. (2017). Intergranular crack during fatigue in Al-Mg-Si aluminum alloy thin extrusions, *Int. J. Fatigue.*, 100, pp. 105–112. DOI: 10.1016/j.ijfatigue.2017.03.028.
- [72] Hojná, A. (2017). Overview of intergranular fracture of neutron irradiated austenitic stainless steels, *Metal*, 7(10), pp. 392. DOI: 10.3390/met7100392.
- [73] Hou, L.G., Xiao, W.L., Su, H., Wu, C.M., Eskin, D.G., Katgerman, L., Zhuang, L.Z., Zhang, J.S. (2021). Room-temperature low-cycle fatigue and fracture behaviour of asymmetrically rolled high-strength 7050 aluminium alloy plates, *Int. J. Fatigue.*, 142, pp. 105919. DOI: 10.1016/j.ijfatigue.2020.105919.



- [74] James, M.N. (2010). Intergranular crack paths during fatigue in interstitial-free steels, *Eng. Fract. Mech.*, 77, pp. 1998–2007. DOI: 10.1016/j.engfracmech.2009.12.006.
- [75] Tian, D.D., Liu, X.S., He, G.Q., Shen, Y., Lv, S.Q., Wang, Q.G. (2016). Low cycle fatigue behavior of casting A319 alloy under two different aging conditions, *Mater. Sci. & Eng. A.*, 654, pp. 60–68. DOI: 10.1016/j.msea.2015.12.023.
- [76] Ma, M., Wang, B., Liu, H., Yi, D., Shen, F., Zhai, T. (2020). Investigation of fatigue crack propagation behavior of 5083 aluminum alloy under various stress ratios Role of grain boundary and Schmid factor, *Mater. Sci. & Eng. A.*, 773, pp. 138871. DOI: 10.1016/j.msea.2019.138871.
- [77] Wen, W., Cai, P., Ngan, A.H.W., Zhai, T. (2016). An experimental methodology to quantify the resistance of grain boundaries to fatigue crack growth in an AA2024 T351 Al-Cu Alloy, *Mater. Sci. & Eng. A.*, 666, pp. 288–296. DOI: 10.1016/j.msea.2016.04.071.
- [78] Fan, K.L., Liu, X.S., He, G.Q., Cheng, H., Zhang, Z. (2015). Influences of strain rate on the low cycle fatigue behavior of gravity casting Al alloys, *Mater. Charact.*, 107, pp. 239–248. DOI: 10.1016/j.matchar.2015.07.024.
- [79] Floweday, G., Petrov, S., Tait, R.B., Press, J. (2011). Thermo-mechanical fatigue damage and failure of modern high performance diesel pistons, *Eng. Fail. Anal.*, 18, pp. 1664–1674. DOI: 10.1016/j.engfailanal.2011.02.002.
- [80] Kouzeli, M., Mortensen, A. (2002). Size dependent strengthening in particle reinforced aluminium, *Acta Mater.*, 50, pp. 39–51. DOI: 10.1016/S1359-6454(01)00327-5.
- [81] Kumai, S., King, J.E., Knott, J.F. (1992). Fatigue crack growth behaviour in molten-metal processed SiC particle-reinforced aluminium alloys, *Fatigue Fract. Eng. Mater. Struct.*, 15, pp. 1–11. DOI: 10.1111/j.1460-2695.1992.tb00011.x.
- [82] Emami, A.R., Begum, S., Chen, D.L., Skszek, T., Niu, X.P., Zhang, Y., Gabbianelli, F. (2009). Cyclic deformation behavior of a cast aluminum alloy, *Mater. Sci. & Eng. A.*, 516, pp. 31–41. DOI: 10.1016/j.msea.2009.04.037.
- [83] Zeng, R.C., Ke, W., Han, E.H. (2009). Influence of load frequency and ageing heat treatment on fatigue crack propagation rate of as-extruded AZ61 alloy, *Int. J. Fatigue.*, 31, pp. 463–467. DOI: 10.1016/j.ijfatigue.2008.07.005.
- [84] Tabibian, S., Charkaluk, E., Constantinescu, A., Szmytka, F., Oudin, A. (2013). TMF-LCF life assessment of a Lost Foam Casting A319 aluminum alloy, *Int. J. Fatigue.*, 53, pp. 75–81. DOI: 10.1016/j.ijfatigue.2012.01.012.